2001

Physiography and Late Quaternary-Holocene Processes of Northeastern Gulf of Mexico Outer Continental Shelf off Mississippi and Alabama

James V. Gardner
University of New Hampshire, Durham, jim.gardner@unh.edu

Peter Dartnell
U.S. Geological Survey

Kenneth J. Sulak
USGS

Brian R. Calder
University of New Hampshire, Durham, brian.calder@unh.edu

Laurent Hellequin
University of New Hampshire, Durham

Gulf of Mexico Science, 2001(2), pp. 132–157

Physiography and Late Quaternary-Holocene Processes of Northeastern Gulf of Mexico Outer Continental Shelf off Mississippi and Alabama

JAMES V. GARDNER, PETER DARTNELL, KENNETH J. SULAK, BRIAN CALDER, AND LAURENT HELLEQUIN

High-resolution multibeam mapping of the mid- and outer continental shelf and upper slope off Mississippi and Alabama reveals a complex bathymetry that reflects conditions during the last eustatic rise and the present high stand of sea level. The most prominent bathymetric features are pinnacles and hardgrounds that are scattered throughout the area. These features generally stand <10 m above the surrounding seafloor, cover large areas, and display a variety of morphologies. Almost all the reef pinnacles and hardgrounds have zones of high acoustic backscatter on their summits and on the seafloor immediately adjacent to their southwest walls. In addition, they also have erosional moats on the seafloor to the southwest. Large fields of bedforms are scattered throughout the mapped area. The asymmetries and orientations of the bedforms suggest that they were formed by excursions of the northeast-flowing Loop Current. In contrast, the pervasive ponding of sediment on the northeast sides of bathymetric highs indicates that one of the predominant directions of sediment transport has been to the south and southwest. The shelf break is a zone of numerous landslides of various sizes and complexities. The morphology of several landslide scars indicates that some of the failures occurred recently. One large reef-capped salt dome was mapped in the area, surrounded by a large field of pockmarks. Fields of pockmarks are also scattered on the shelf. The growth and demise of the reefs are related to the fluctuating transgression of eustatic sea level during the last deglaciation. Two episodes of reef drowning are correlated with the increased rates of sea-level rise during documented melt-water pulses; the first occurred from 14.8 to 14.2 ka and the second from 11.8 to 11.2 ka. Rates of sea-level rise exceeded the maximum growth rate of hermatypic corals only during these two intervals since the last glacial maximum and thus drowned the coral communities.

The outer continental shelf of the northeastern Gulf of Mexico south of Mississippi and Alabama (Fig. 1) is an area of intense use, principally by energy companies and commercial fishing. Concerns arose during the 1980s and 1990s about anthropogenic effects on the habitats that support benthic fish communities in this area. This region contains known deep-water reefs that provide fish havens, key spawning sites, and habitats for early larval and juvenile stages of economically important sport/food fishes. In addition, deep-water reefs function as a key source of repopulation of already heavily affected inshore reefs. However, it is not known to what extent the shelf physiography interacts with and possibly controls biological differentiation because the shelf bathymetry is so poorly known (Schroeder et al., 1997). Consequently, a major research effort was launched in the early 1990s to map this portion of the outer continental shelf principally by use of conventional 100-kHz sidescan sonar (Laswell et al., 1990; Sager et al., 1992) and a 72-kHz bathymetric sidescan sonar system called TAMU^2 (Hilde et al., 1991). Subsequently, new technologies emerged during the mid-1990s that allowed the generation of much more quantitative views of the seafloor bathymetry than the older systems. In particular, high-resolution multibeam echosounders (MBES) now available can generate geodetic-quality bathymetry as well as coregistered and precisely georeferenced calibrated acoustic backscatter (Hughes Clarke, 1996; Gardner et al., 1999, 2000a).

The purpose of this paper is to provide the first detailed quantitative description of the geomorphology of the outer shelf and upper slope south of Mississippi and Alabama derived from high-resolution MBES mapping surveys conducted in 2000 and to discuss the late Quaternary and Holocene processes that are reflected in the geomorphology.

Previous Studies

Ludwick and Walton (1957) published the first reconnaissance survey of the geomorphology of the outer shelf in the study area. They used seismic-reflection profiling and discovered what they termed "pinnacles," features that rise several meters above an otherwise flat outer shelf. Ludwick (1964) expanded the earlier study to include an investigation of the sediments on the entire northeasten Gulf of Mexico shelf. The pinnacles were interpreted as early transgressive bioherms that grew vertically as sea level rose (Ludwick and Walton, 1957; Ludwick, 1964). These studies generated little but academic interest until the 1980s, when environmental concerns began to focus research on these features. Laswell et al. (1991, 1994) mapped the area with conventional sidescan sonar and a high-frequency subbottom profiler. They identified and mapped the distribution of reef–like mounds, ridges, and pockmarks. Hardgrounds and pinnacles have also been described on the inner shelf (Schroeder et al., 1988; Fleischer and Schroeder, 1998). Sager et al. (1992) correlated the control of bioherm growth with the last eustatic transgression as initially proposed by Ludwick and Walton (1957). McBride and Byrnes (1995) presented a detailed bathymetric map based on historical bathymetric data from NOAA and discussed the morphology of the area interpreted from these data. Several studies have described the shallow acoustic stratigraphy of the area (Kindinger, 1988, 1989; Laswell et al., 1991; Sager et al., 1999).

Description of Multibeam Systems

The sidescan sonars (SSS) used during the late 1980s and early 1990s (Laswell et al., 1991, 1994) provided the first views of the geomorphology of the seafloor in the pinnacles area, but these systems have several disadvantages with respect to MBES systems for accurately mapping the seafloor. The disadvantages fall into four categories: lack of accurate bathymetric data, poor georeferencing, absence of the ability to calibrate backscatter, and geometric problems with aspect ratio. A conventional SSS signal contains bathymetric information only at nadir and as the presence of bathymetric highs and lows as revealed by zones of shadows (i.e., no data). The SSS displays and/or digitizes the received energy as a simple time series of seafloor returns to the transducer. The first return is recorded first, regardless of where on the seafloor it has come from, then the second return, and so on to form a narrow stripe of returns perpendicular to the ship track. This scheme works reasonably well on a flat seafloor where sequential returns are progressively farther from the ship track, but if the seafloor has relief, then the sidescan representation incorporates geometric errors in feature locations because the sequence of returns no longer fits the time-distance progression. The seafloor relief need not be more than a few meters for significant geomorphic misrepresentations to occur. The misrepresentations are exacerbated by a procedure commonly used in conventional SSS of "correcting" slant range to ground range by simple geometry that uses the height of the sidescan fish above the seafloor as one side of a right triangle and assumes that the slant range is the straight line hypotenuse to a flat seafloor. This procedure omits corrections for both seafloor relief and the curved acoustic raypaths caused by changes in water-column sound speed.

Accurate georeferencing requires the determination of a precise latitude and longitude for each data pixel in the sidescan record. Accurate determination of pixel location is made extremely difficult with a conventional SSS because the sonar sensor is typically towed an estimated range and azimuth behind the ship and the sonar typically has no motion sensors to determine pitch, roll, and yaw. Consequently, at best, the position of the fish is estimated with an unknown precision. The assignment of georeferencing to each pixel leads to ambiguities that introduce undetermined errors, especially at high resolutions.

Given the lack of calibrated acoustic backscatter, any given sediment facies can have a wide range of backscatter levels, and the backscatter levels from any given facies can, and typically do, dynamically change throughout the SSS survey. The conventional SSS of the 1980s and 1990s constantly scaled the amplitude of the received acoustic energy by an automatic gain control (AGC) so as to maximize the dynamic range of the received signals to the full dynamic range of the sonar-recording system, which in a digital system is typically 12 bits/sample. The recorded dynamic range was then reduced to 4 or 8 bits for graphical display. However, because the AGC scaling was not logged; the actual acoustic energy of the received signal for a given sediment facies and the relative acoustic backscatter energies could not be compared between facies. In addition, the energy level of the outgoing pulse was not recorded, so that the received energy could

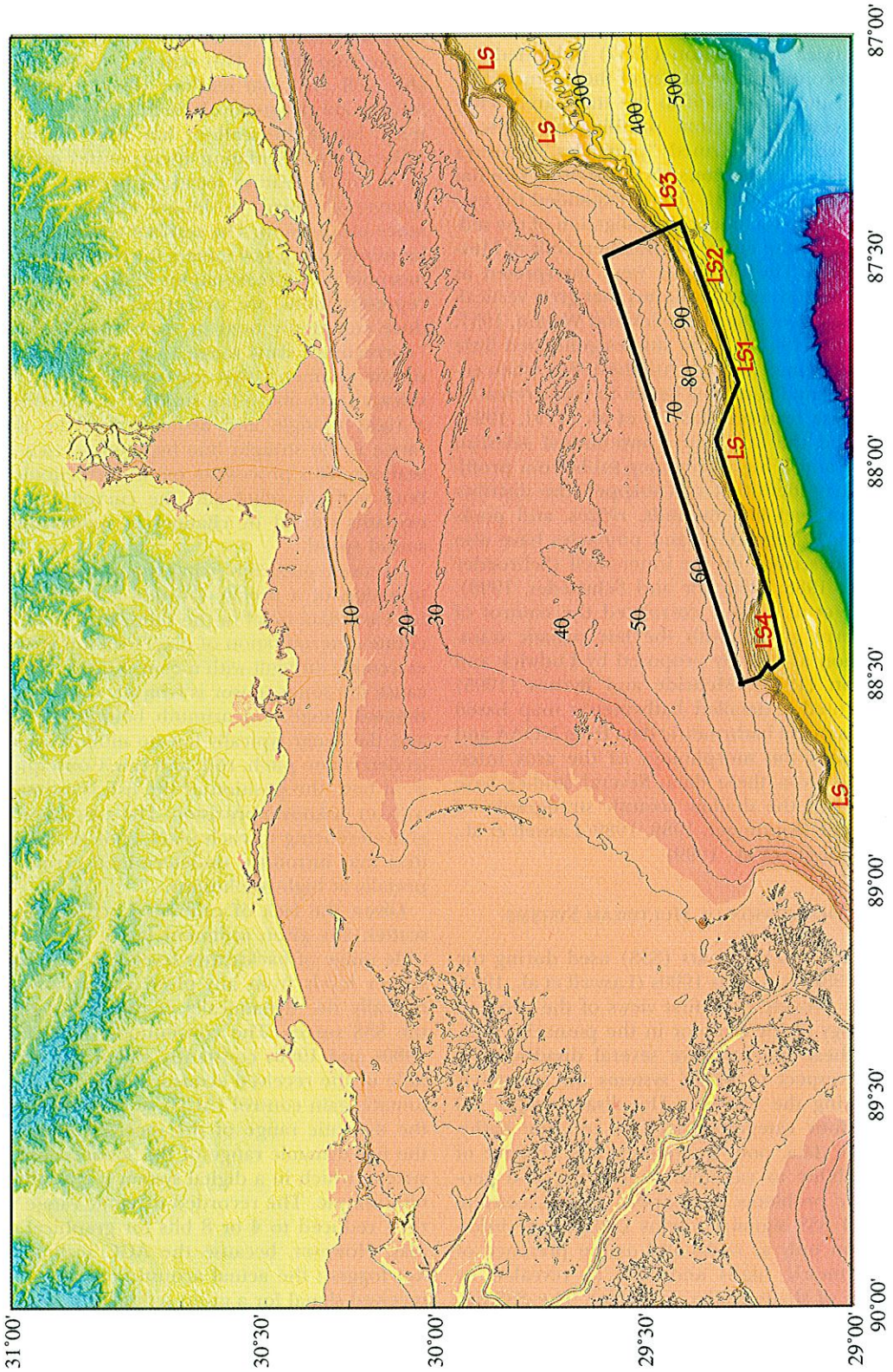
LS
LS1
LS2
LS3
LS4
10
20
30
40
50
60
70
80
90
100
400
500
87°00'
87°30'
88°00'
88°30'
89°00'
89°30'
90°00'
31°00'
30°30'
30°00'
29°30'
29°00'

not be referenced to the transmitted energy. This prevented the determination of the relationship between transmitted and received source levels so that the responses of different SSS systems could not be compared over the same piece of seafloor.

The fourth problem with conventional SSS, especially before the 1990s, is that the transmit and record rates are fixed but the distance traveled during the receive cycle constantly varies. Until the late 1990s, navigation was not accurate enough to precisely determine the distance covered during each receive cycle. This results in variable data density and an aspect ratio that can be, depending on survey speed, as large as 3:1 (footprint length along track vs. footprint length across track). This aspect ratio distorts the image geometry of features on the seafloor. The method typically used to partially correct aspect ratio was to replicate a swath of pixels in the along-track direction to generate a square footprint.

The studies of the area in the late 1980s and early 1990s recognized problems that accompany conventional sidescan sonars, and later studies used the bathymetric sidescan sonar TAMU[2] to map small areas in the study area (CSA and TAMU, 1999). There is very little published information about TAMU[2], but the system did provide both acoustic backscatter and bathymetry data (see examples of TAMU[2] data over pinnacles of the outer shelf in Fig. 2). For comparison, the same area shown in Figure 2 was extracted from the high-resolution MBES data and is shown in Figure 3. Notice that the aspect ratio of the images in Figures 2 and 3 are different. This is a result of poor georeferencing of the TAMU[2] data, as discussed above. Also notice the poor correlation in pattern and backscatter level of the TAMU[2] backscatter data (Fig. 2A) with that of the multibeam data (Fig. 3A), although the frequencies are similar. One difference is that the TAMU[2] backscatter is uncalibrated, whereas the MBES backscatter is calibrated. These examples are in no way meant to criticize the earlier studies; they are shown simply to demonstrate the improvement in technology that occurred with the introduction of high-resolution MBES with calibrated signals, inertial motion sensors, navigation, and high-speed computers. In fact, the systems used in studies by Sager et al. (1992) were remarkably successful at locating and describing many of the major features on this outer shelf and slope.

A detailed description of high-resolution MBES mapping systems can be found in Hughes Clarke et al. (1996) and Gardner et al. (2000). Two high-resolution MBES systems were used in this study. Each multibeam system included an inertial motion sensor, a dual differential global positioning system (GPS) navigation system, and a water-column sound-velocity profiler. Most of the area was mapped with a Kongsberg Simrad EM1002 MBES. The EM1002 system operates at frequencies of 98 kHz (inner ±50° swath centered at nadir) and 93 kHz (the outer ±20°). The system transmits a narrow along-track, wide across-track pulse and then receives backscattered energy from 111 2° × 2° receive apertures that are distributed across track. Some of the area was mapped with a Kongsberg Simrad EM1000 MBES that operates at a 95-kHz frequency and uses 60 receive apertures. Digital GPS–aided inertial navigation was used for both cruises resulting in position accuracies of all the bathymetric soundings to within ±1 m, and depth accuracies of 0.05% of the water depth for both systems. Each of the ~500 million bathymetric soundings has a corresponding coregistered acoustic-backscatter-energy level calibrated to the energy of the transmitted pulse at 1 m out from the transducer.

Regional Setting

The study area includes the middle and outer continental shelf and uppermost continental slope south of Alabama and Mississippi, directly east of the Mississippi Delta and immediately west of the head of De Soto Canyon (Fig. 1). The mapped area lies immediately east of the Lower Cretaceous shelf break, which defines the eastern boundary of the northern Gulf of Mexico salt province (Martin, 1978; Diegal et al., 1995). In general, the shelf is a relatively broad, smooth, surface that gently slopes seaward from the coast to the 40-m isobath with a gradient that ranges from 0.51° immediately east of the Mississippi River outlet to a gradient of 0.03° at its broadest due south of Mississippi. The shelf gradient steepens at the 40-m isobath to gradients that range from

←

Fig. 1. Digital bathymetric map of the continental shelf (data from http://www.navo.navy.mil/ngli). Contour interval 10 m to 150-m isobath, then 50 m beyond. Pinnacles area outlined. Landslides labeled LS (see text for discussion).

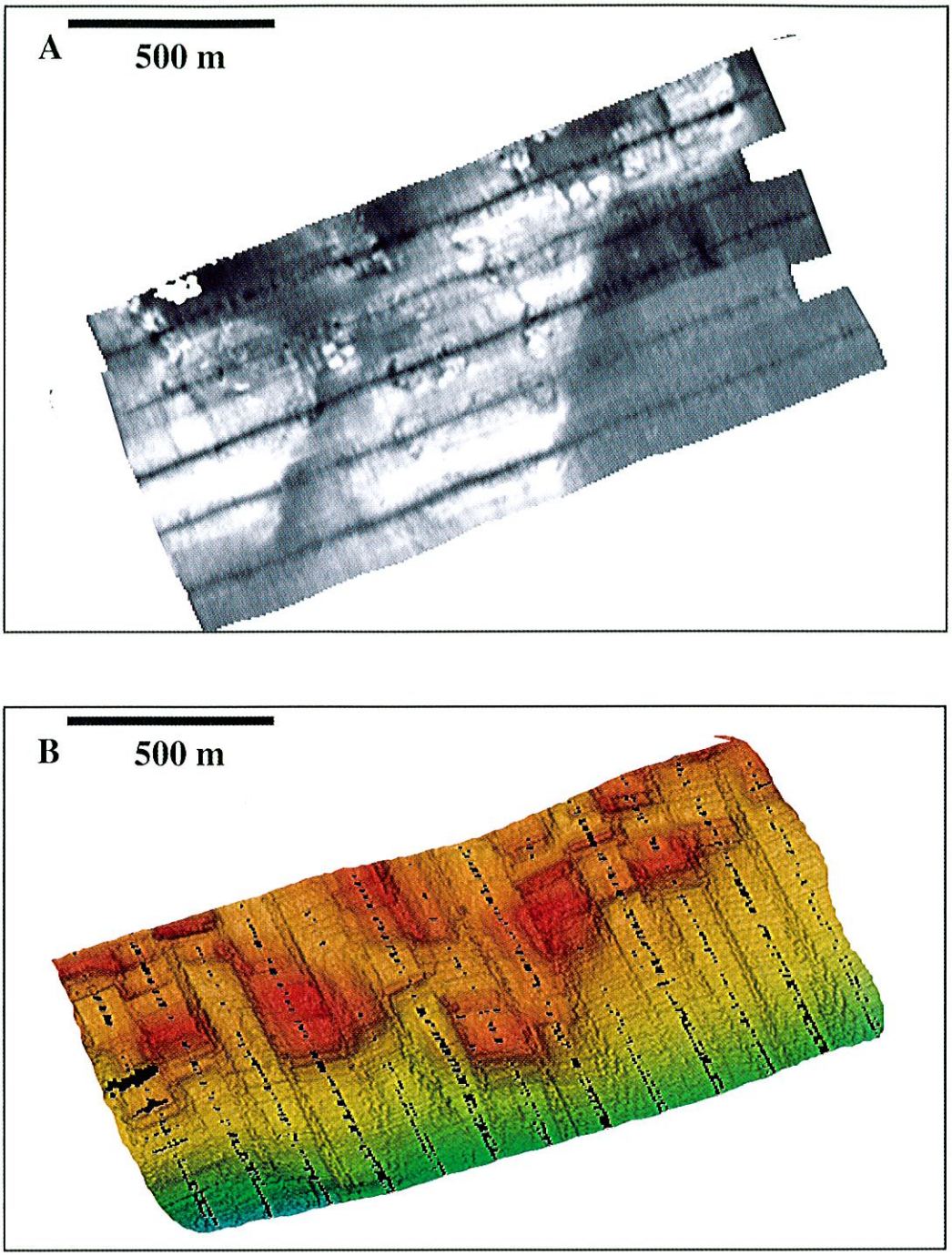

Fig. 2. Examples of TAMU[2] data from an area of the outer shelf. (A) Backscatter data: light tones are high backscatter, and (B) colored shaded relief of same area. Notice the rectilinear shapes and track-parallel orientation (the black gaps) of the positive-relief features in the bathymetry. See Figure 4 for location. Data courtesy of Texas A&M University.

~0.03° to 1.2° from the 40- to the 90-m isobath. The shelf break is an abrupt transition from shelf gradients to upper-slope gradients that range from 0.53° to >5°. The shelf break has been modified by a series of broad reentrants that have more gentle transitions between the outer shelf and upper slope.

Surficial sands blanket most of the mid and outer shelf and represent transgressive fluvial sediment deposited during last eustatic rise (Ludwick, 1964). Fine-grained silt and clay have been transported to the shelf in this area by the Mississippi River to the west and, to lesser degrees, by the Pascagoula, Mobile, Pearl, and Apalachicola Rivers to the north (Mazzullo and Bates, 1985). Fine quartz sand has also been supplied by these rivers, but the sands are a mixture derived from two distinctly different provinces; the central continental United States (via the Mississippi River) and the Appalachian Mountains (via rivers to the east; Mazzullo and Bates, 1985). A zone of calcareous muds occurs along the outermost shelf and includes a narrow belt of reef and interreef carbonates (Ludwick, 1964). McBride and Byrnes (1995) described three shelf-margin lobes that they relate to low-stand fluvial systems, two of which are described in greater detail by Sager et al. (1999). The later study concluded that one delta was deposited during a eustatic regression and the other during the succeeding transgression.

The oceanic circulation in the area is dominated by periodic eddies off the anticyclonic Loop Current that flows along the continental slope south of the study area and by seasonal cyclones that progress north and northwestward through this part of the northeastern Gulf of Mexico. Although the main core of the Loop Current is south of the study area, the seafloor has been influenced by periodic excursions of the current and its eddies (Vokovich, 1988). Surface current speeds as fast as 60 cm/sec have been observed on the slope between the Mississippi Delta and De Soto Canyon (Molinari and Mayer, 1982). Periodic hurricanes pass through the area generating cyclonic northeasterly wind >100 knots that have the potential for significant influence on the surficial sediments in the study area.

Outer Shelf Bathymetry

The area mapped (Fig. 1) covers ~50% of the outer shelf between the Mississippi River delta to the west and De Soto Canyon to the east. The MBES survey resulted in two maps of the outer shelf and upper slope, a detailed bathymetric map, and a coregistered acoustic-backscatter map (Figs. 4 and 5, respectively). The bathymetry of the outer shelf is complex, including areas of scattered pinnacles and hardgrounds, some of which rise >10 m above the surrounding seafloor; large fields of bedforms; scarps, and ridges, some with >5 m of relief; a salt dome; large tracts of pockmarks; and shelf-edge landslide scars and slumps.

Pinnacles and hardgrounds.—The outer shelf in this region is called "the Pinnacles Area," following Ludwick and Walton (1957), who discovered, mapped, and sampled a belt of calcareous reefs with several meters of relief. Similar deep-water reefs have been described elsewhere on the outer shelf of the northern Gulf of Mexico (Trowbridge, 1930; Shepard, 1937; Carsey, 1950; Gealy, 1955; Parker and Curray, 1955; Sager et al., 1992; Benson et al., 1997; Gardner et al., 1999). Pinnacles, or more properly, reef pinnacles, are easily identified in the MBES data as relatively small, isolated bathymetric highs with very high acoustic backscatter (−18 to −21 dB) (Fig. 6). The term "hardgrounds," following the usage by Schroeder et al. (1988), is used here for a seafloor feature with a hard or indurated surface, regardless of origin or relief. Hardgrounds typically appear on the MBES data as slightly elevated regions (up to several meters of relief) with very high backscatter (−18 to −23 dB) relative to the surrounding seafloor (−28 to −31 dB) (Fig. 6). There is a gradation between a pinnacle and a hardground that ranges from a single small pinnacle (type 1) to a group, sometimes coalesced, sometimes solitary, of relatively large flat-topped pinnacles (type 2), to a smooth-topped, relatively high hardgrounds (type 3) to a rough-topped, relatively low hardgrounds (type 4) (Fig. 6). Sediment has ponded on the northeast side of most hardgrounds producing a pronounced, steep, step down of >1 m toward the southwest. In addition, most pinnacles of type 1, 2, and 3 have a seafloor depression, typically ~1 m deep, immediately to their southwest. A few hardgrounds appear to be completely buried by a thin veneer of sediment. Because pinnacles and hardgrounds commonly occur associated with one another, they have been mapped as a single unit (Fig. 7). Pinnacles and hardgrounds are found throughout the mapped area, and are concentrated between the 65- and 125-m isobaths. In addition, pinnacles and hardgrounds are more common in the eastern half of the area, where they occur in shallower depths. Groups of pinnacles and hardgrounds

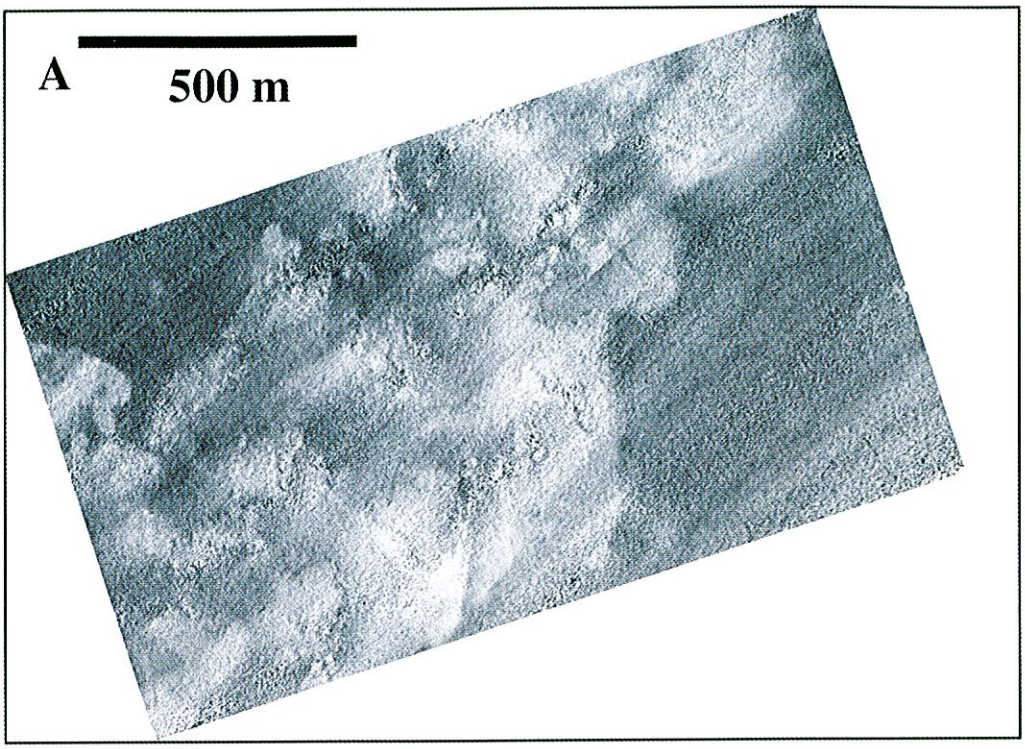
A
500 m

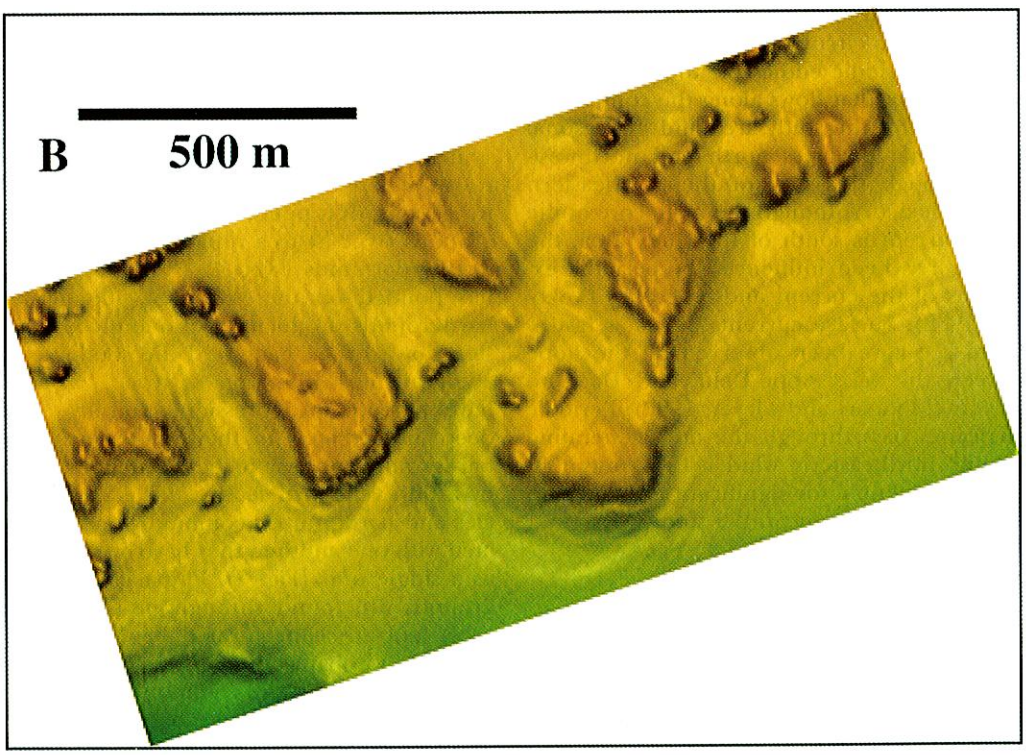
B
500 m

commonly trend parallel to isobaths (as observed by Sager et al., 1992), but several groups occur with no apparent relation to bathymetric trends. Pinnacles associated with hardgrounds more commonly occur on the margin than on the middle of the hardground, producing a rim effect. Only a few pinnacles rise 10 m above the hardground surfaces.

Sager et al. (1992) presented two sidescan-sonar images of what they identified as "patch reef" and "reef-like mound" (called here "hardground"). Figure 8 is the MBES bathymetry and acoustic backscatter from the area of one of their images. The MBES images show a clear difference between a patch reef (type 4) and a reeflike mound (types 2 and 3). A typical patch reef is composed of a very rough area composed of hundreds to thousands of small (<2 m high) pinnacles per square kilometer. The small pinnacles cover several tens of square kilometers and are scattered over the area between the 50- and 100-m isobath. By comparison, a hardground typically is a slightly elevated platform that can vary in area from small (<0.2 km^2) to large (>50 km^2), with groups of pinnacles that rise from the platform surface. However, the distinction may be arbitrary because patch reefs may simply be hardgrounds that are buried by a thin veneer of sediment.

The summits of all hardgrounds and pinnacles have high backscatter and, in addition, the seafloor immediately southwest of the southwestern wall of all hardgrounds and most relatively large pinnacles also display high backscatter (−18 to −30 dB) (Fig. 9). The depressions, or moats, on the seafloor southwest of the hardgrounds and pinnacles are mantled by high backscatter (>−23 dB) material (Fig. 9).

Bedforms.—Extensive fields of sediment bedforms are found in the northeastern and north-central portions of the mapped area and smaller fields are found scattered throughout the area (Fig. 10). All of the bedforms fall within the dune classification of Ashley (1990). The bedforms group into four types on the basis of bedform geometry.

A large field of sinuous-crested asymmetric bedforms (Fig. 11A) occurs in the north-central part of the area. The trends of the bedforms range from N40W to N80W, with wave heights that range from 70 to 100 cm and wavelengths that range from 200 to 400 m. The stoss sides of the bedforms face southwest. The crest of each bedform has higher backscatter (−29 dB) than the adjacent the trough (−32 dB). This bedform field covers at least 100 km^2 of shelf and may extend much farther to the north outside the study area. An area of enigmatic depressions is associated with this bedform field (Fig. 11B). The depressions are 2–5 m deep and have horizontal dimensions of hundreds of meters wide and long, with west faces consistently steeper (2.2° to >3°) than their east faces (1.2°–2°). The long axes of the depressions trend about N20W, slightly oblique to the adjacent bedform trends.

Straight-crested symmetrical bedforms group into two classes on the basis of wavelength. Straight-crested symmetrical bedforms with wavelengths >100 m (Fig. 11C) are located directly south of the large field of asymmetrical bedforms. These have wave heights of up to 0.5 m, and their crest orientations are north-south, roughly perpendicular to the isobaths. This field covers ~24 km^2 of the shelf. There is no acoustic-backscatter difference between trough and crest on these bedforms. Another type of straight-crested symmetrical bedforms occurs in the eastern portion of the mapped area. These bedforms have wavelengths <100 m and wave heights <0.5 m (Fig. 11D). This field covers ~42 km^2 of seafloor. These bedforms also have no acoustic-backscatter difference between trough and crest.

Fields of straight-crested, asymmetrical (stoss side facing northwest) bedforms occur in the eastern portion of the mapped area. These bedform types only occur on the south and southwest side of hardgrounds and pinnacles, have very straight to slightly curved crests that trend N20E for several kilometers, and have very high acoustic backscatter (−25 dB) on the crests and low backscatter (−31 dB) in the troughs. These bedforms have wavelengths ~100 m and wave heights ~0.5 m.

Ridges.—A prominent ridge occurs in the middle of the mapped area that roughly follows the 65-m isobath for 20 km, then jumps to the 69-m isobath and follows it for an additional 18 km (Fig. 12). The ridge was interpreted by

←

Fig. 3. Examples of Simrad EM1002 MBES data from same area as shown in Figure 2. (A) Backscatter image with same convention as Figure 2. (B) Shaded relief: notice that the seafloor features are much better resolved and lack the rectilinear artifacts seen in Figure 2. See Figure 4 for location.

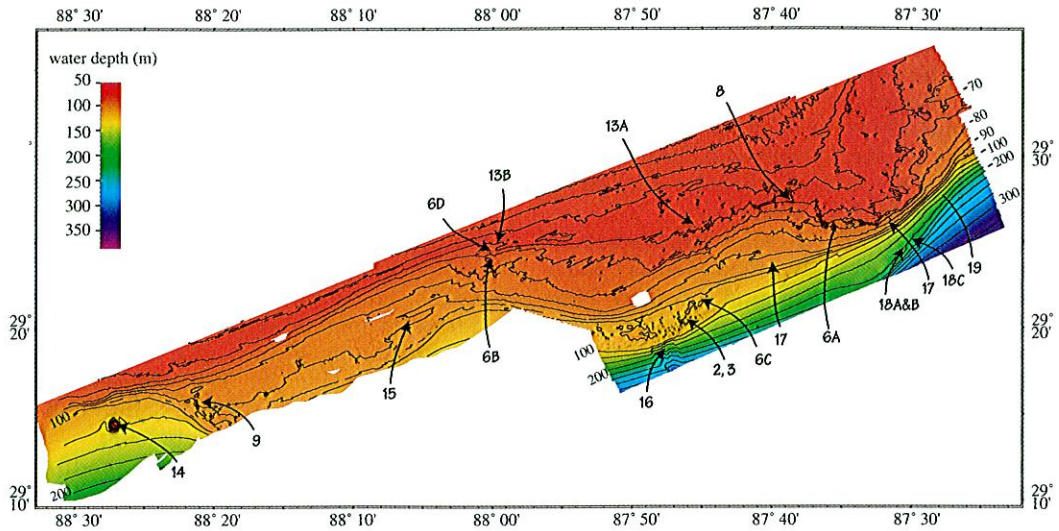

Fig. 4. Color shaded-relief map of outer shelf and slope from MBES data. Contour interval on slope is 25 m offshore of shelf break and 10 m on the shelf. Numbered arrows point to location of figures.

Sager et al. (1992) as a submerged lithified low-stand barrier island or longshore bar. The ridge rises as much as 8 m above the surrounding seafloor. Close-up views of the ridge show that it is composed of a series of ridges and swales that make up a 350- to 400-m-wide feature (Fig. 13). The seafloor to the north and northeast of the ridge is consistently ~4 m shallower than the seafloor to the south and southwest. As with the pinnacles and hardgrounds, a 1- to 2-m deep moat parallels the ridge on its south side (profile in Fig. 12). The ridge and a 500-m wide zone on the seafloor immediately to the southwest have higher backscatter values of (−26 dB) compared with the ridge (−32 dB). The continuity of the ridge is broken only where it makes a major change in trend where it breaks up into a zone of pinnacles and hardgrounds (Fig. 13A).

Salt domes.—One piercement salt dome is found in the western-most mapped area (Fig. 12). This salt dome was previously mapped with a narrowbeam echosounder by Gittings et

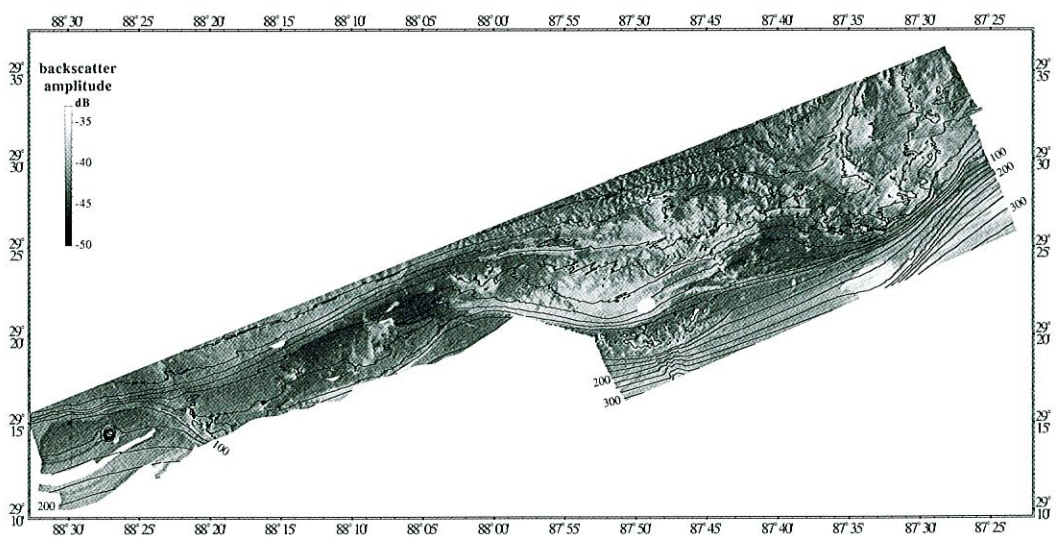

Fig. 5. Acoustic-backscatter map of outer shelf and slope from MBES data. Light tones are higher backscatter. Contour interval on slope is 25 m to shelf break and 10 m on the shelf. See Figure 4 for locations.

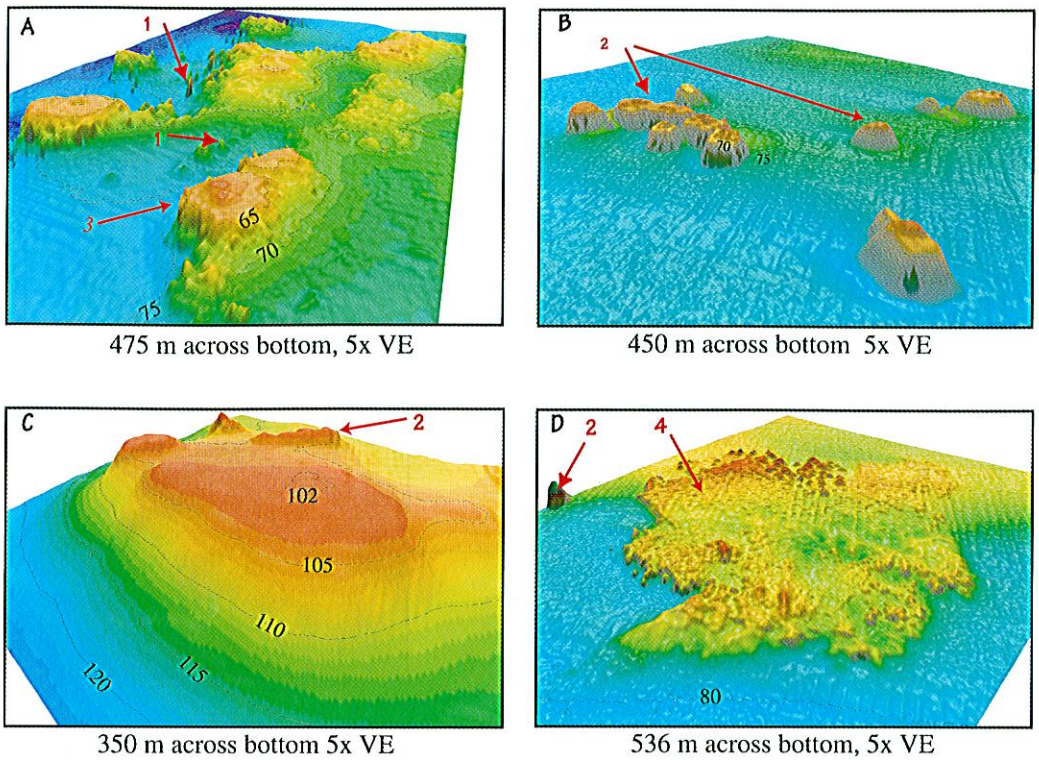

Fig. 6. Color-shaded relief oblique views of selected pinnacles and hardgrounds. (A) Raised hardgrounds with examples of solitary pinnacles (type 1), (B) solitary to coalesced relatively large flat-topped pinnacles (type 2), (C) smooth-topped, relatively high hardground (type 3), and (D) relatively low hardground (type 4). Location of figures shown with numbered black arrows on Figure 7.

al. (1990). The salt dome is capped by an extensive reef and has a moat around its base, and a pockmark field immediately to the north (Fig. 14). The salt dome is slightly elliptical in plan, with a north-south diameter of 1.6 km and an east-west diameter of 1.4 km. There is a 300-m long spur on the north side that projects from the base of the dome. The sides of the dome are smooth and convex in profile. The salt dome rises ~60-m above the seafloor with an additional 20-m thick reef constructed on its summit. A 10-m deep, 200- to 500-m wide moat surrounds the base of the dome with a 40-m wide, 1-m deep outlet channel that leads from the southwest edge of the moat and can be followed downslope for >8 km.

Pockmarks.—Fields of pockmarks related to gas and/or fluid expulsion are found scattered throughout the western half of the mapped outer shelf and upper slope (Fig. 12). These features are identical to the pockmarks described by Hovland and Judd (1988) in their classic work. Individual pockmarks vary in size up to ~20 m in diameter at their upper rim and ~1 m deep with a typical pockmark density of 10 pocks per 1000 m^2 (Fig. 15). The occurrence of pockmarks is not surprising because of the extensive deposits of oil and gas found in this region, but we were unable to locate published references detailing their distribution.

Landslides and slumps.—At least eight large landslides and landslide scars occur along the shelf break (Fig. 1). The landslide scars are identified by a change in shelf-break gradient that coincides with a reentrant in the trend of the shelf break. The landslide scars range in size from <3 km to >18 km across and have cut back the slope by as much as 8 km. One example of a landslide scar (Laswell et al., 1990) is located at 29°18.4′N, 87°47.5′W (LS1 in Fig. 1; Fig. 16). The head of this scar is 2.9 km across, and the failure surface is 2.6 km long. The landslide removed a 15-m thick sediment mass, which indicates that 0.05–0.1 km^3 of sediment has been displaced. The floor of the failure scar is very irregular, with large blocks scattered on the surface and a drainage

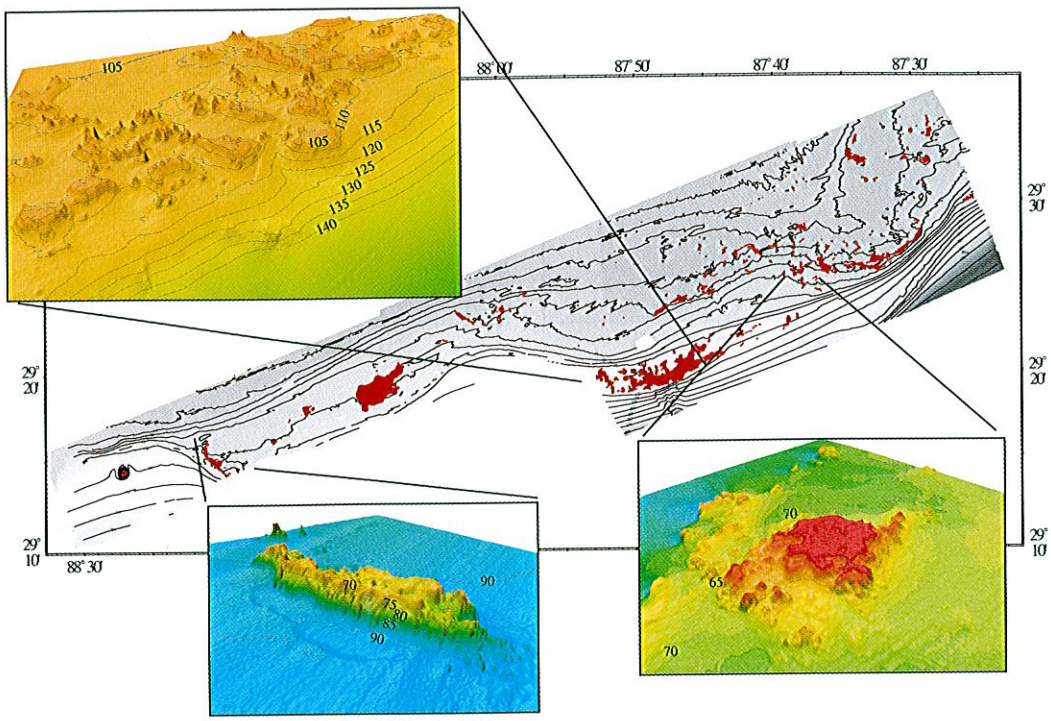

Fig. 7. Distribution of pinnacles and hardgrounds (red areas). Insets show oblique views of examples of pinnacles and hardgrounds.

pattern that was established after the failure. The presence of large blocks was confirmed with remotely operated vehicle video runs (R.V. *Tommy Munro* cruise USGS 2001-01). The acoustic backscatter from the floor of the scar differs little from that of the surrounding upper slope. The southern boundary of the high-resolution MBES data occurs just below the landslide scar where a 100-m wide, 4-m deep channel leads out of the scar, trending south. The high-resolution MBES data were merged with available NOAA digital bathymetry (NOAA, 1998) to reveal the full extent of the channel (Fig. 16B).

A prominent landslide scar is found just below the shelf break along a 14-km section of the uppermost slope (LS2 in Fig. 1, Fig. 17A). The landslide scar is ~600 m wide and 10 m deep, which indicates ~8.4×10^4 m^3 of sediment was transported downslope from this area. A series of five bathymetric highs that strike perpendicular to the slope occur 2 km east of the western terminus of the failure. The bathymetric highs are up to 800 m long, rise as much as 5 m above the slope, and have 2- to 3-m deep moats on their western sides (Fig. 17), with backscatter values of −25 dB, compared with the surrounding seafloor values of −30 dB.

A series of large failures occurs immediately downslope of landslide LS2. The largest one (Fig. 18A) is 7 km along shelf, 3 km across shelf, and has ~2 m of relief, representing ~4.2×10^4 m^3 of displaced sediment. This feature has higher acoustic backscatter (−21 dB) than the surrounding nondisturbed areas (−26 dB) (Fig. 18B). The feature appears to be a slump (Fig. 18C) that possibly represents material transported from the shelf-edge landslide.

Another series of five large slumps occurs along an 8-km long zone of the upper slope, 11 km east of the large slump (LS3 in Fig. 1, Fig. 19). These slumps vary in size from 1.5 to 2.0 km wide and ~1.5 km long, with ~10 m of relief. Each slump has a pronounced 3- to 4-m deep moat on its southwest margin. A striking linear double-furrow scar bisects the westernmost of these slumps and abruptly terminates on its southeast side. The double-furrow scar trends N45E for >6.5 km in an extremely straight course with furrows 1–2 m deep. The slumps may represent debris transported by the shelf-edge landslides. The southwestern-

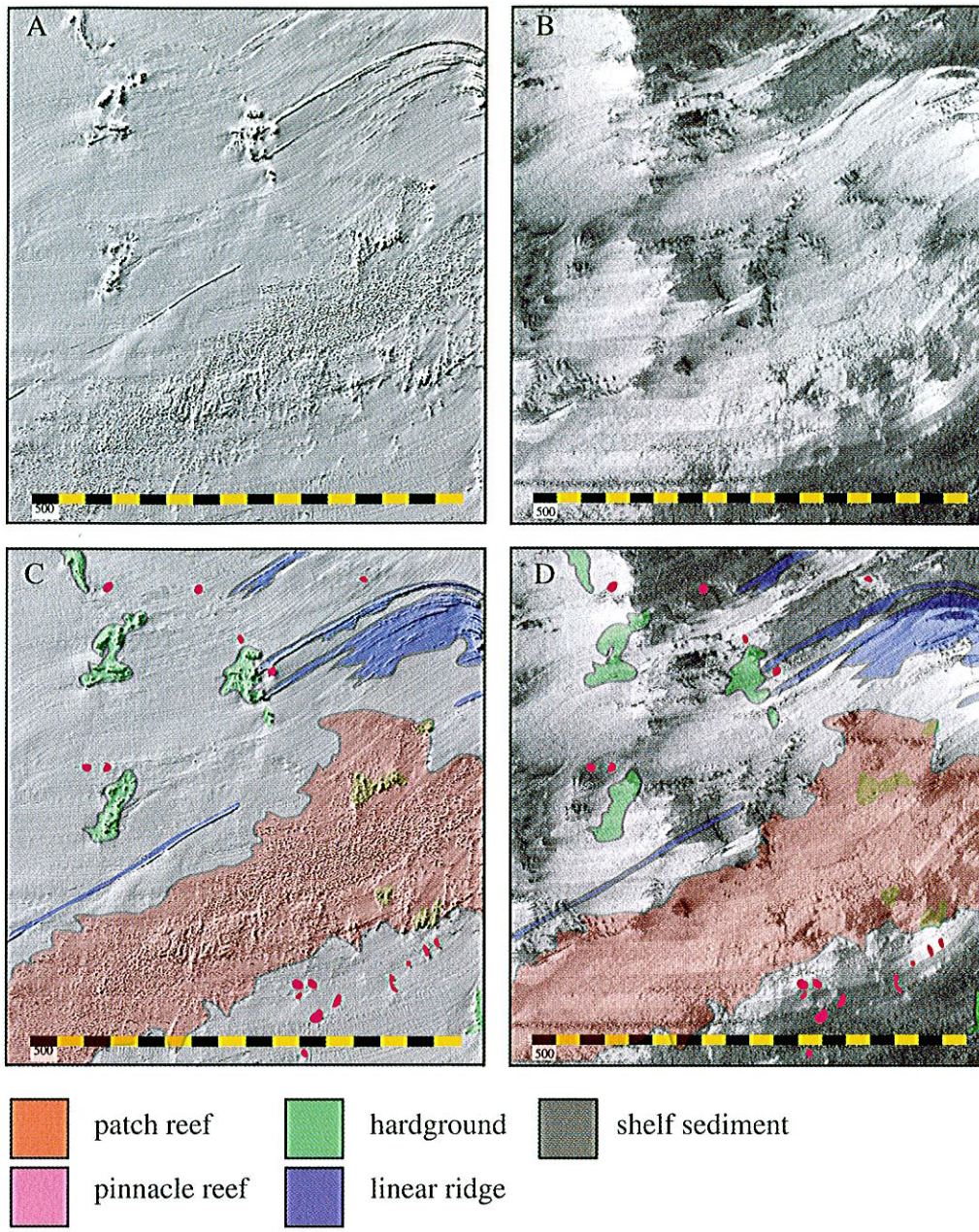

Fig. 8. Example of map view of shaded-relief (A) and coregistered calibrated acoustic backscatter (B) of area of patch and pinnacle reefs, hardgrounds, and linear ridges. (C) Interpretations of panel A. (D) Interpretation superimposed on backscatter image. Notice on backscatter image (B) that smooth area northwest of mapped patch reef apparently is thinly sediment-covered hardground. See Figure 4 for location.

most slump looks the freshest of the four and has the highest backscatter (−21.8 dB). The sharpness of bathymetric detail and backscatter level decrease with distance to the northeast, suggesting an age progression from northeast to southwest.

A large reentrant in the shelf on the western end of the mapped area may also be two coalesced landslide scars. The reentrant occurs along the shelf break, but its physiography is very different from the scars described above. This scar (LS2 in Fig. 1), has a broad, smooth floor that is 24 km across and has cut 8 km back into the shelf. The eastern border of the

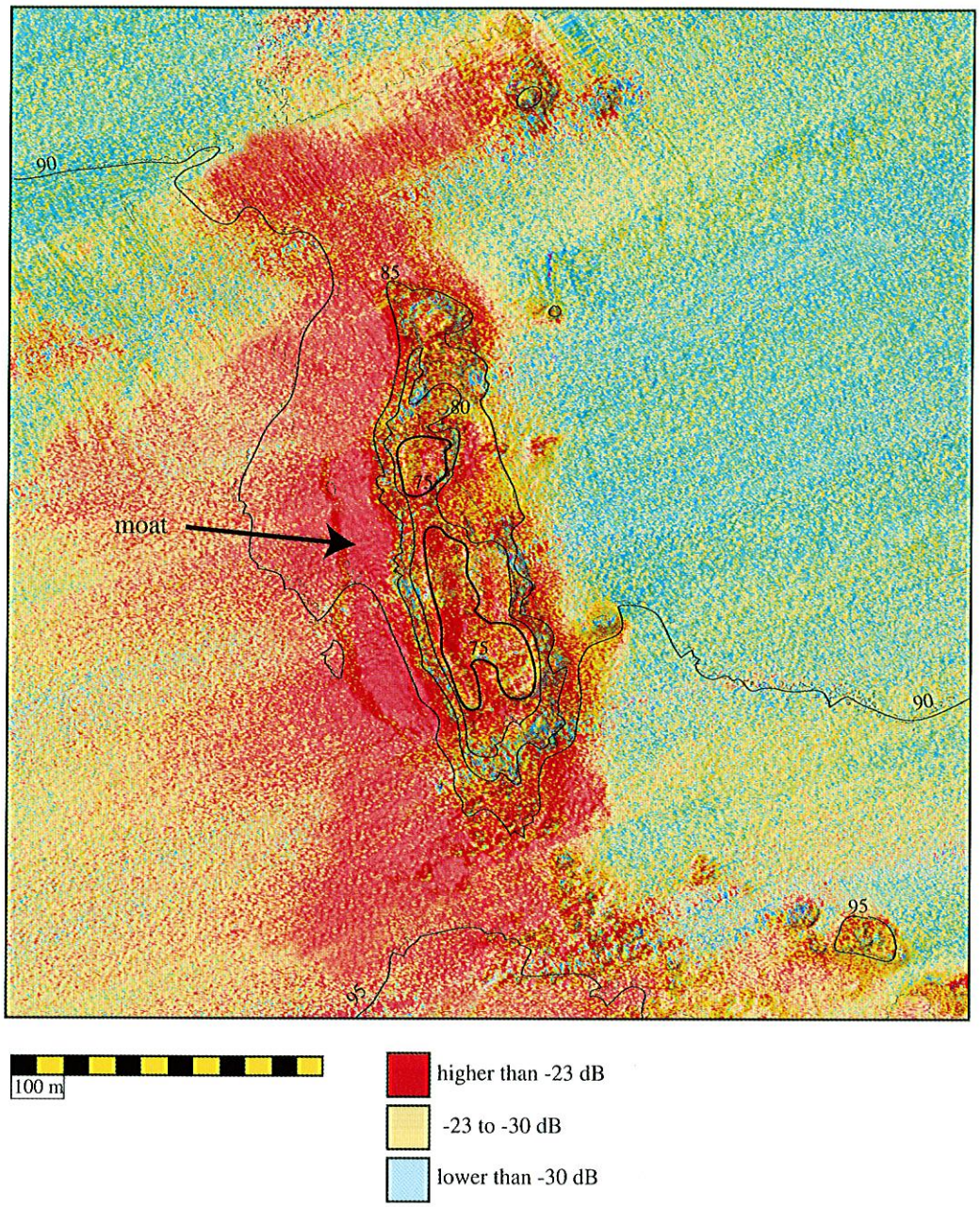

Fig. 9. Color-coded acoustic backscatter map of a prominent reef. Note moat and high-backscatter zone on southwest side of feature. See Figure 4 for location.

reentrant coincides with the trend of the Lower Cretaceous shelf (Martin, 1978; Diegal et al., 1995) and may represent a major structural trend through the area. However, if the reentrant is a landslide scar, then a sediment mass >100 m thick has been removed, which indicates that at least 19 km^3 of material may have been transported downslope over time. The acoustic backscatter within the reentrant is ~3 dB lower than that of the adjacent outer shelf. A salt dome (described above) rises from the center of this scar, apparently associated with the field of salt domes that occurs to the south in water depths of 1000–2000 m (Diegal et al., 1995). The lack of slide blocks, displaced sediment masses, and other associated landslide

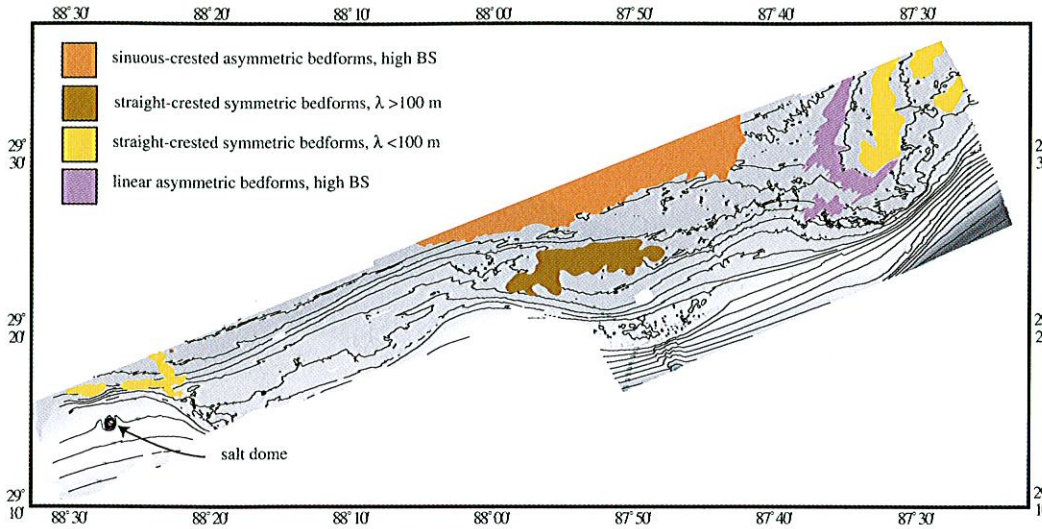

Fig. 10. Map showing distribution of bedforms types. BS, acoustic backscatter. See text for discussion.

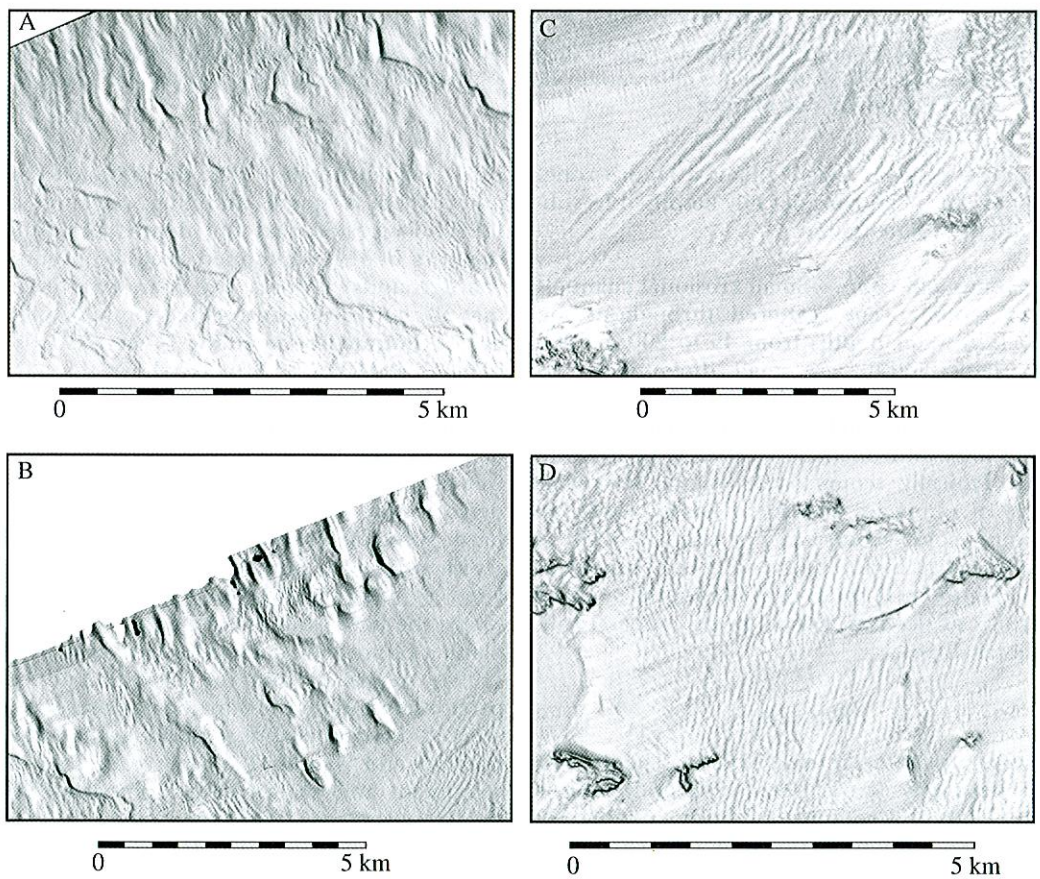

Fig. 11. Shaded-relief maps of various classes of bedforms. (A) Sinuous-crested asymmetric bedforms, (B) enigmatic depressions, (C) large straight-crested symmetrical bedforms, and (D) small straight-crested symmetrical bedforms. All maps illuminated from 45° elevation, 315° azimuth.

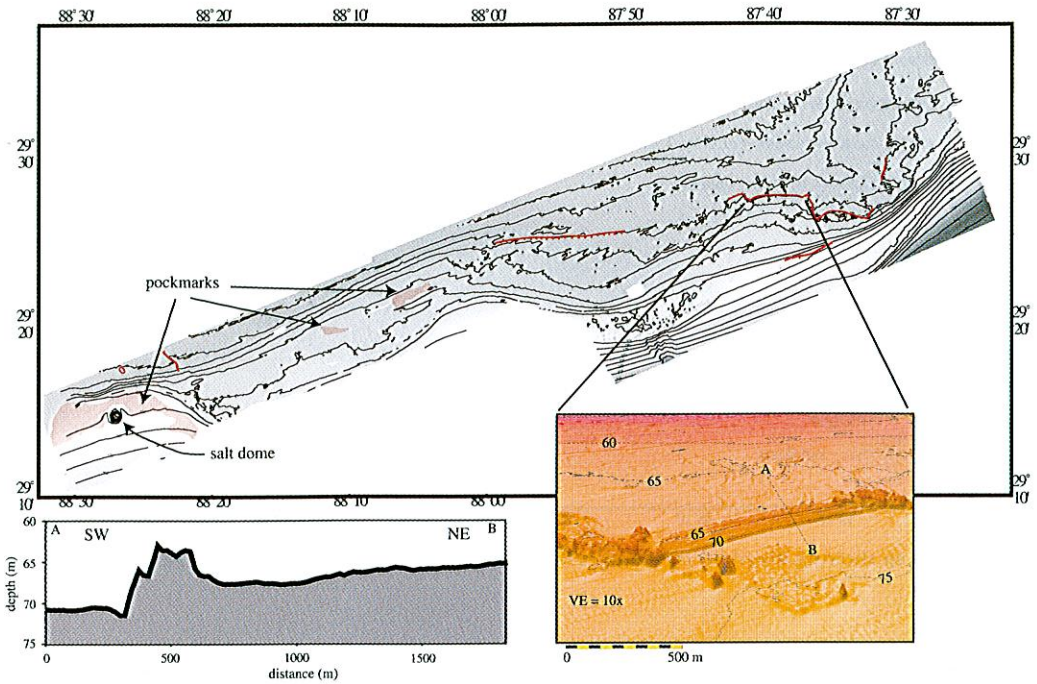

Fig. 12. Map showing distribution of linear ridges, salt dome, and pockmarks. Inset shows oblique view of a linear ridge. Profile A–B shows difference in elevation interpreted as sediment ponded on NE side and erosional moat on SW side of ridge.

features suggests that if this is a failure zone, then it has been considerably modified by subsequent sedimentation.

Channels and scours.—Small erosional channels and scours occur scattered throughout the area, in water depths from 45 to 200 m. The channels typically are small, disconnected to one another, and vary in width up to 200 m with <2 m of relief. Scours invariably are depressions with one side steeper than the others. Typically, scours occur on the southwest side of pinnacles and some hardgrounds, although some scours are not associated with a bathymetric high. Scours are not confined to the continental shelf; they are found in water depths as deep as 200 m on the upper continental slope.

Discussion

Features related to the transgression.—The present physiography of the outer shelf and slope is the result of a complex interplay of processes that have influenced this region since at least the last eustatic low stand. Samples from pinnacles contain few living hermatypic corals (Gittings et al., 1990; Sager et al., 1992) and rare calcareous algae (Ludwick and Walton, 1957), which suggests that the pinnacles are relict. From a sparse sampling, Sager et al. (1992) suggested that the depths of all the summits of the flat-topped reef-like mounds (hardgrounds) occur at the 66-m isobath and that all the flat-topped reeflike mounds might be concentrated between the 74- and 82-m isobaths. The MBES bathymetry shows the hardgrounds are found in a wide range of water depths (107–66 m), and there is no consistent depth to their top surfaces. Reef pinnacles are usually associated with hardgrounds, which underscores the tendency of corals to colonize on hard substrates rather than unconsolidated sediment. Those pinnacles that appear unrelated to hardgrounds may simply be cases where the hardgrounds have been buried by a blanket of post-lowstand sediment. Sager et al. (1992) suggested that the hardgrounds are patch reefs and that linear ridges represent cemented barrier islands and longshore bars. Ludwick and Walton (1957) correlated the development and growth of the pinnacles with the last eustatic sea-level transgression. Sager et al. (1992) speculated that the pinnacles may have grown during periods of faster eustatic rise and hardgrounds (what they termed "shallow mounds") may have developed during a short sea-level stasis.

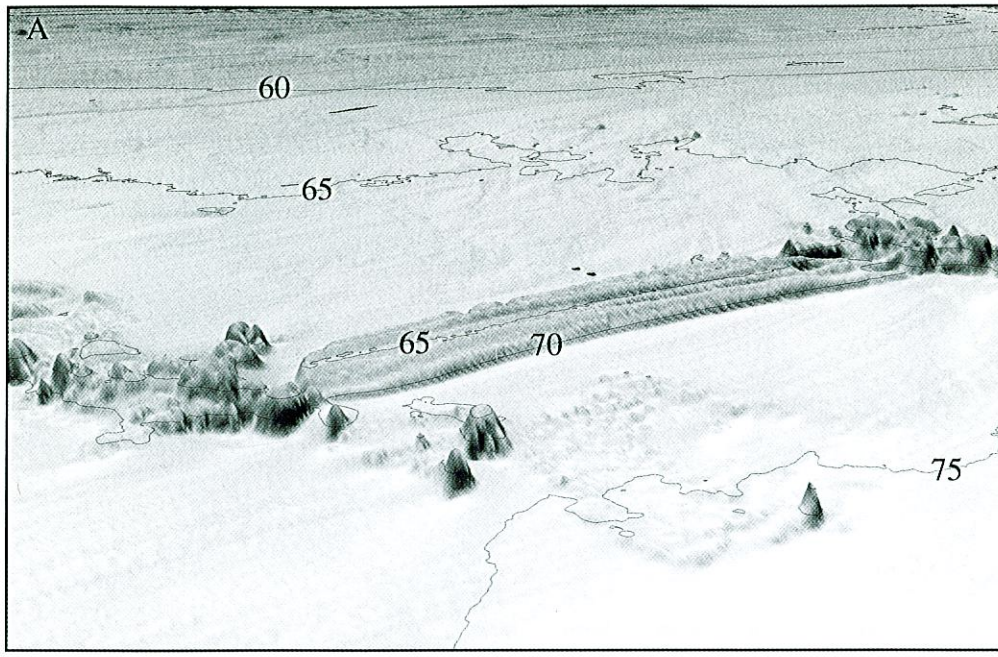

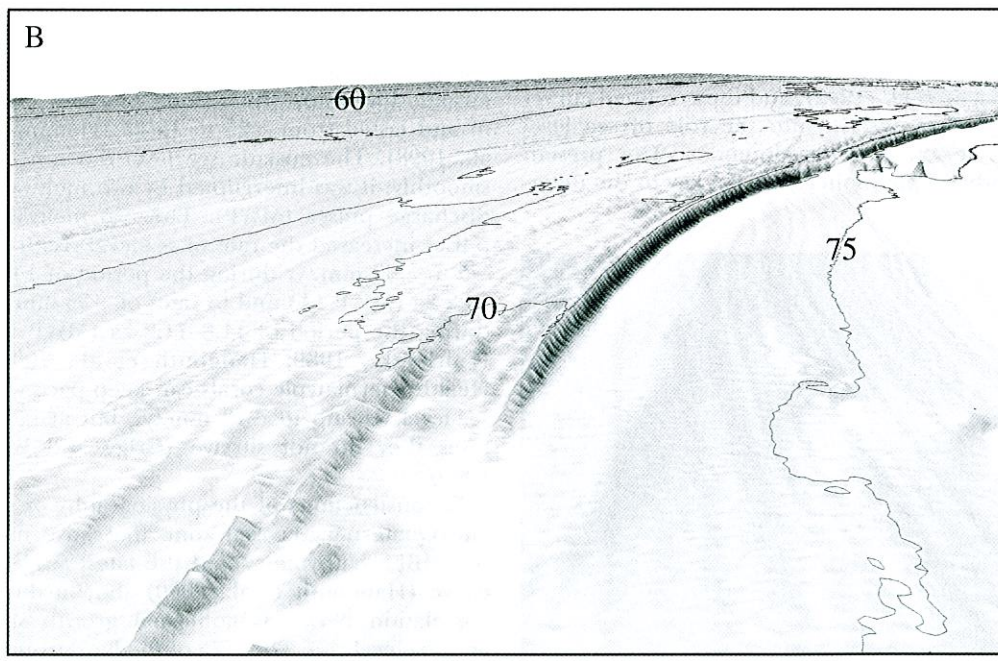

Fig. 13. Oblique views of shaded relief of two segments of ridge shown in inset of Figure 12. Contour interval 5 m, illumination from 45° elevation, 315° azimuth. See Figure 4 for location. Both views looking northeast.

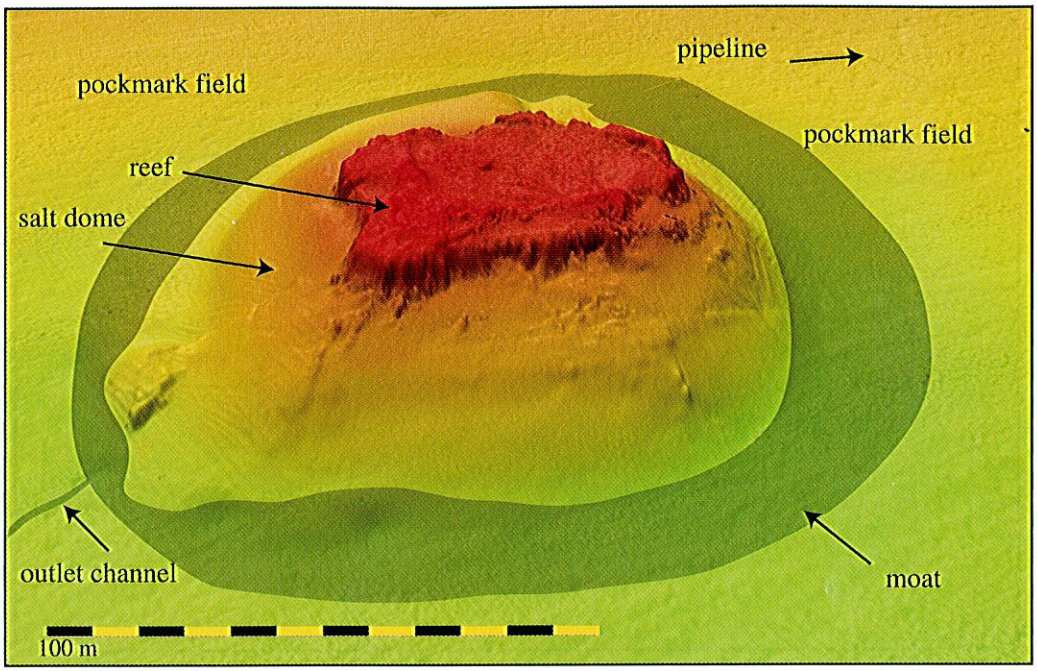

Fig. 14. Oblique color shaded relief with interpretation of reef constructed on top of salt dome. View is looking north, shading elevation 45°, azimuth 315°. See Figure 4 for location.

More detailed sea-level curves for the last transgression (Fairbanks, 1989; Hanebuth et al., 2000) have been developed since the work of Sager et al. (1992), and these refined curves allow clear insight into the role of sea level change on reef development. The present depths of the bioherms are a key to the determination of the relationship between biohermal growth and eustatic sea level. The entire continental shelf was emergent during the last eustatic lowstand, which stood at about −115 m and lasted from ~25 to 19 ka (Fleming et al., 1998). The eustatic sea level did not rise smoothly; it was interrupted by two meltwater discharge pulses (MWP). The two meltwater pulses increased the rate of sea-level rise from ~5 to ~50 mm/yr during the period of 14.8–14.2 ka (MWP 1A) and to rates of ~35 mm/yr during the period of 11.8–11.2 ka (MWP 1B) (Fairbanks, 1989; Hanebuth et al., 2000). Healthy hermatypic corals can keep pace with sea-level rise up to ~10 mm/yr, but at faster rates they do not survive (Grigg and Epp, 1989).

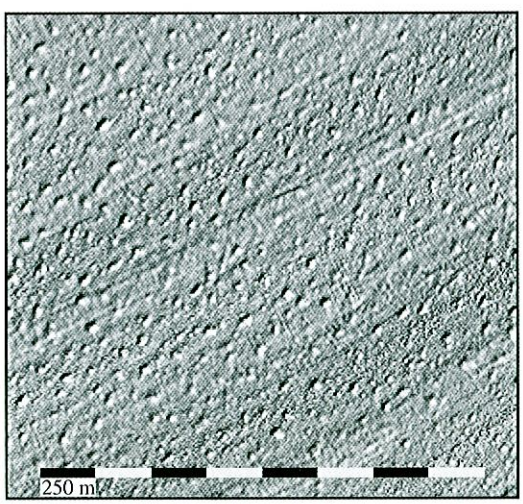

Fig. 15. Shaded relief map view of field of pockmarks. View is looking north, shading elevation 45°, azimuth 315°. See Figure 4 for location.

Reconstructions of the physiography of the late Quaternary coastal zone that have used the MBES bathymetry and the latest sea-level curve (Hanebuth et al., 2000) show a direct correlation between biohermal growth style and sea-level rise. The area of the hardgrounds and pinnacles was subaerial at ~20 ka (Fig. 20A), and because the pinnacles and hardgrounds are composed of marine shells, they must be younger than 20 ka. The first stage of the transgression occurred from ~19 to 14.5 ka, when the initial rate of eustatic rise was ~5

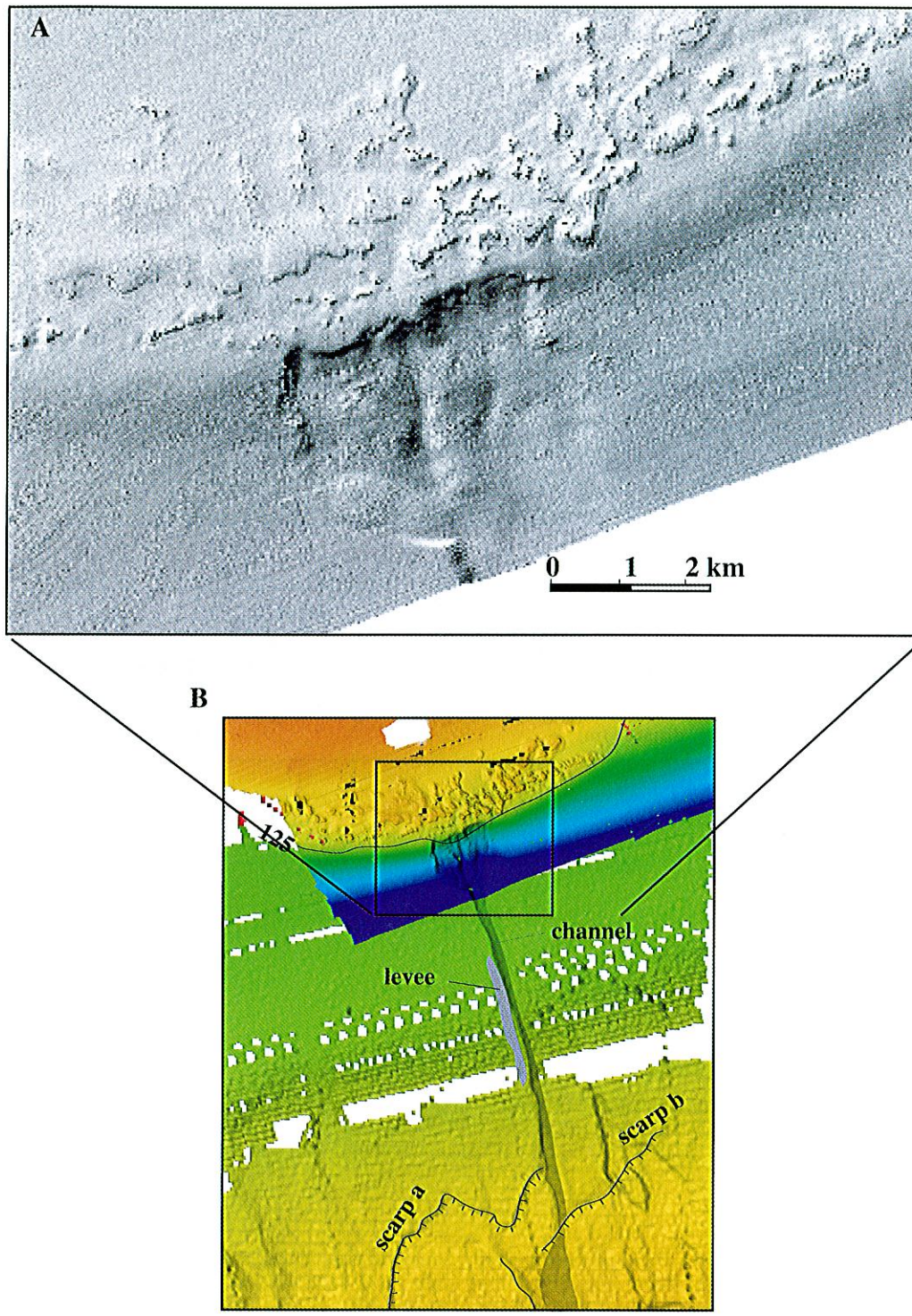

Fig. 16. (A) Shaded relief map view of large landslide scar at shelf break (LS1 on Fig. 1). Note pinnacles and hardgrounds constructed out to the shelf edge, but not beyond. (B) Smaller scale view of color-coded shaded relief combining data from USGS cruise and existing publically available bathymetry. Note the continuation of the linear channel, as well as the levee, and seaward-facing scarps. Relief on scarp "a" is 35 m, and scarp "b" is 20 m.

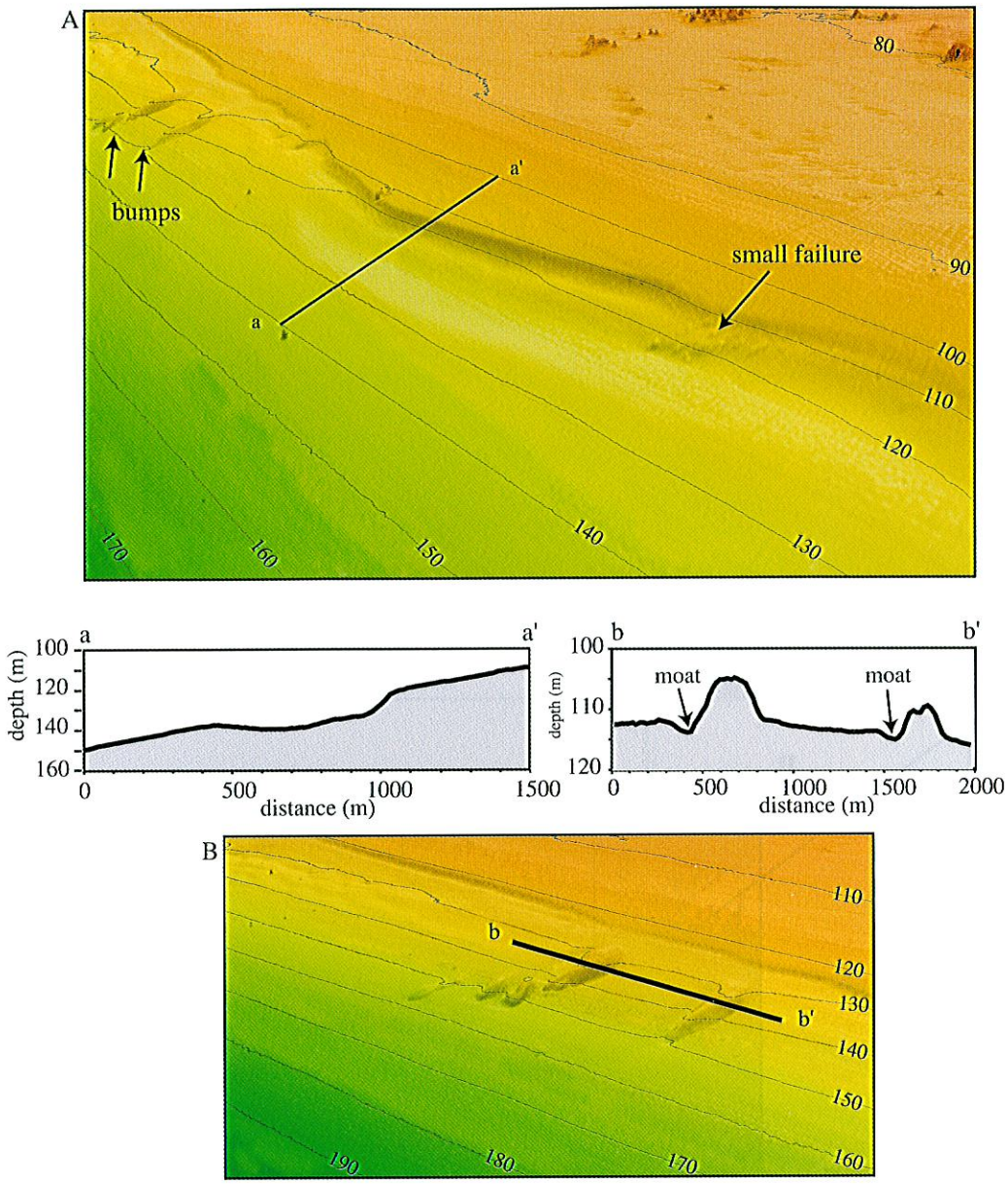

Fig. 17. (A) Color-coded oblique shaded relief views of area of large shelf-edge landslide scar (Fig. 1, LS2) and (B) bumps (buried hardgrounds ?) seen in A. Profiles a-a′ and b-b′ show scale of relief of features. See Figure 4 for location. Scale across bottom of image A is 4.5 km and scale across bottom of image B is 3.0 km.

mm/yr. Water depths of the outermost shelf would have been <15 m deep (Fig. 20B). The slow eustatic rate during this 4.5-ky period, transgressing from today's 120 m to the 95-m isobath, probably would have promoted the development and lateral growth of reef platforms and hardgrounds, because the entire reef surface could have kept pace with the slow eustatic rise. Then, starting at 14.5 ka and lasting until 14.2 ka, MWP 1A, transgressing from today's 95 m to the 87-m isobath, increased the eustatic rise to rates of ~50 mm/yr. Initially, reef pinnacles could have developed at this time, keeping pace with the rapidly rising photic zone. However, eventually the rapid eustatic rise caused by MWP 1A would have outpaced

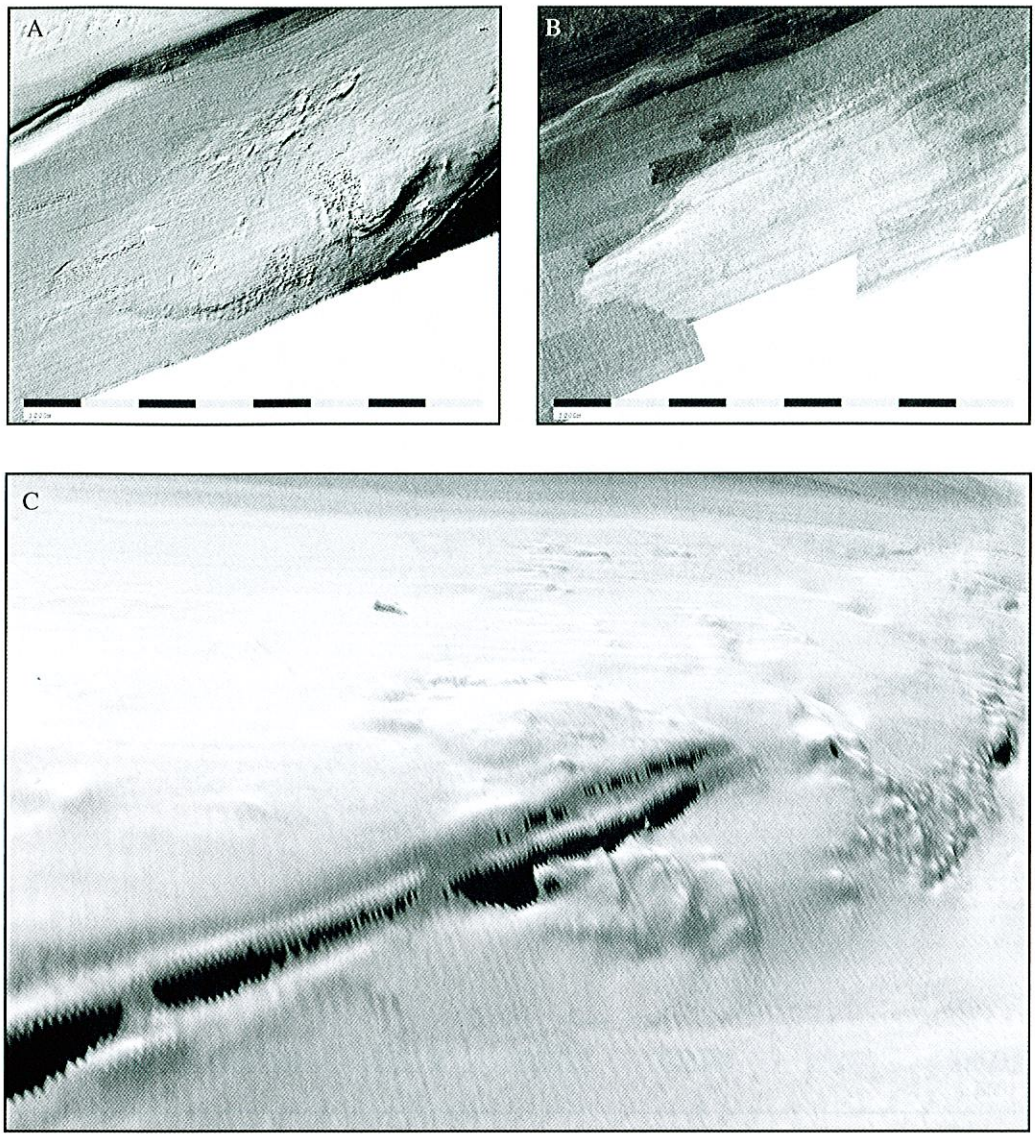

Fig. 18. Map views of shaded relief (A) and acoustic backscatter (B) of large landslide on upper slope (LS2 on Fig. 1). Notice very high backscatter (−21 dB) of landslide compared to adjacent seafloor (−26 dB). (C) Oblique shaded-relief view of landslide mass immediately to the northeast of landslide in Figure 18A that has been disrupted by some unknown process that produced a linear double furrow. View looking northeast. See Figures 4 and 19 for location. Scale across bottom of image is 3.4 km.

vertical coral growth, and the reefs would have drowned. By the end of MWP 1A, the hardgrounds on the outermost shelf would have been at ~30 m depth, the maximum depth for most hermatypic corals (Grigg and Epp, 1989). Although the outermost shelf reefs were drowned during MWP 1A, the midshelf reefs had yet to be established because this area was still 5–10 m above sea level (Fig. 20C).

The rates of eustatic rise slowed to <10 mm/yr for 2,400 yr after MWP 1A. This was the period of establishment and growth of reefs and hardgrounds on the midshelf (Fig. 20C). Hardgrounds were well developed during this interval in northeastern part of the mapped area. The deeper portion of 69-m ridge was at the shoreline at 14 ka, and the ridge was only 8–13 m deep by the end of this period of slow

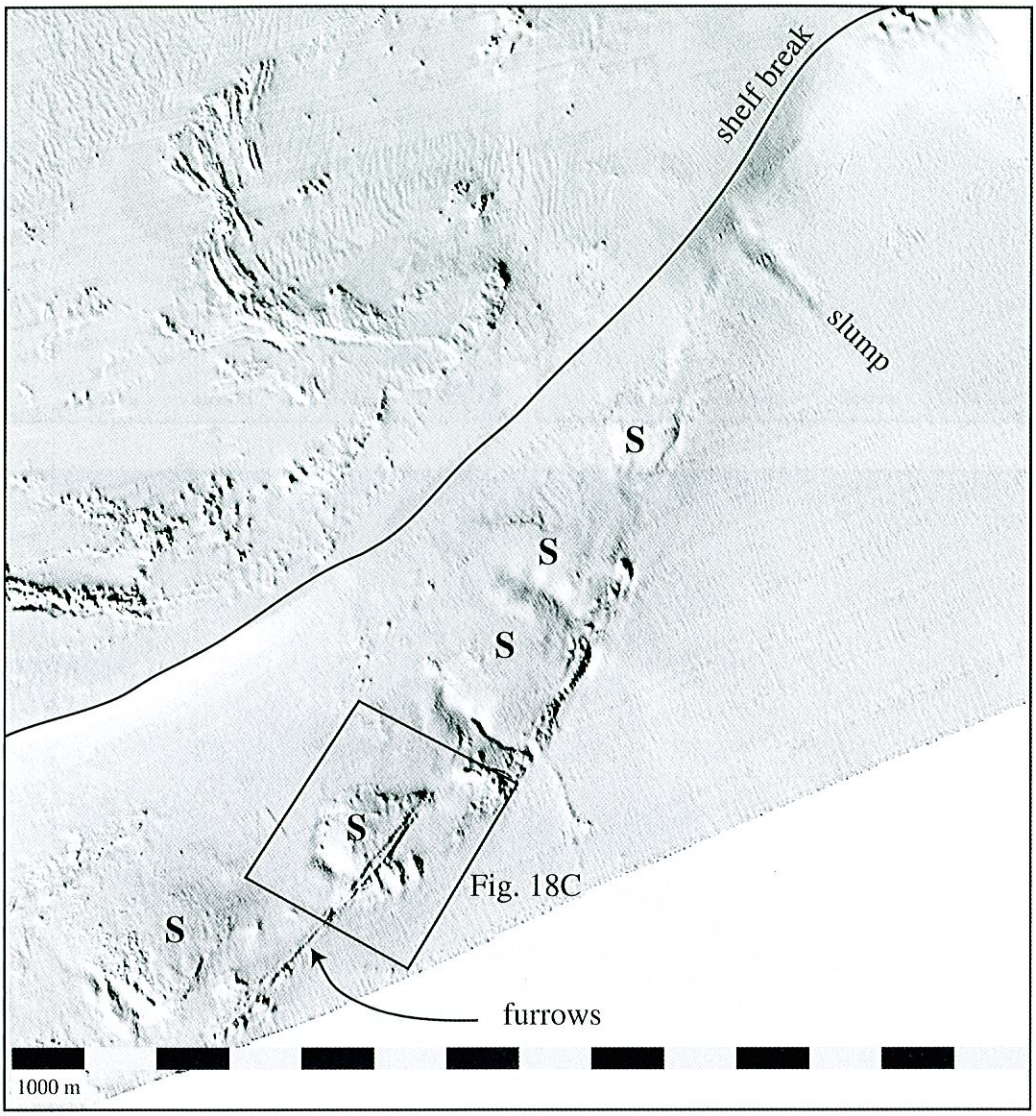

Fig. 19. Map view of shaded relief of portion of outer shelf and slope (LS3 on Fig. 1). Notice isolated pinnacles, hardgrounds, bedforms, and ridges north of the shelf break and the prevalence of slumps south of the shelf break. S, slump. See Figure 4 for location.

sea-level rise at 12 ka. The reef that sits on the summit of the salt dome in the western part of the mapped area probably began to form around 12.5 ka in water depths <5 m, when eustatic sea level was at today's −60-m isobath.

The second melt-water pulse, MWP 1B, occurred between 11.8 and 11.2 ka and increased the rate of eustatic rise to ~35 mm/yr (Fairbanks, 1989). This increased rate of sea-level rise would have drowned reefs developed along today's 53–50-m isobaths, during the preceding period (Fig. 20D). By 11 ka, the entire study area was submerged by at least 5–10 m of water (Fig. 20E). Only a small portion in the northeast section would have been susceptible to reef growth, but there are no indications of hardgrounds or pinnacles in this area.

There are few obvious examples of subaerial features found on the shelf, other than possibly the remnants of channels found in the northern portion of the mapped area. Sager et al. (1992) suggested that the linear ridges are midtransgressive, cemented barrier islands or longshore bars and that the deeper hardgrounds are earlier transgressive bioherms. If the hardgrounds are products of the last low

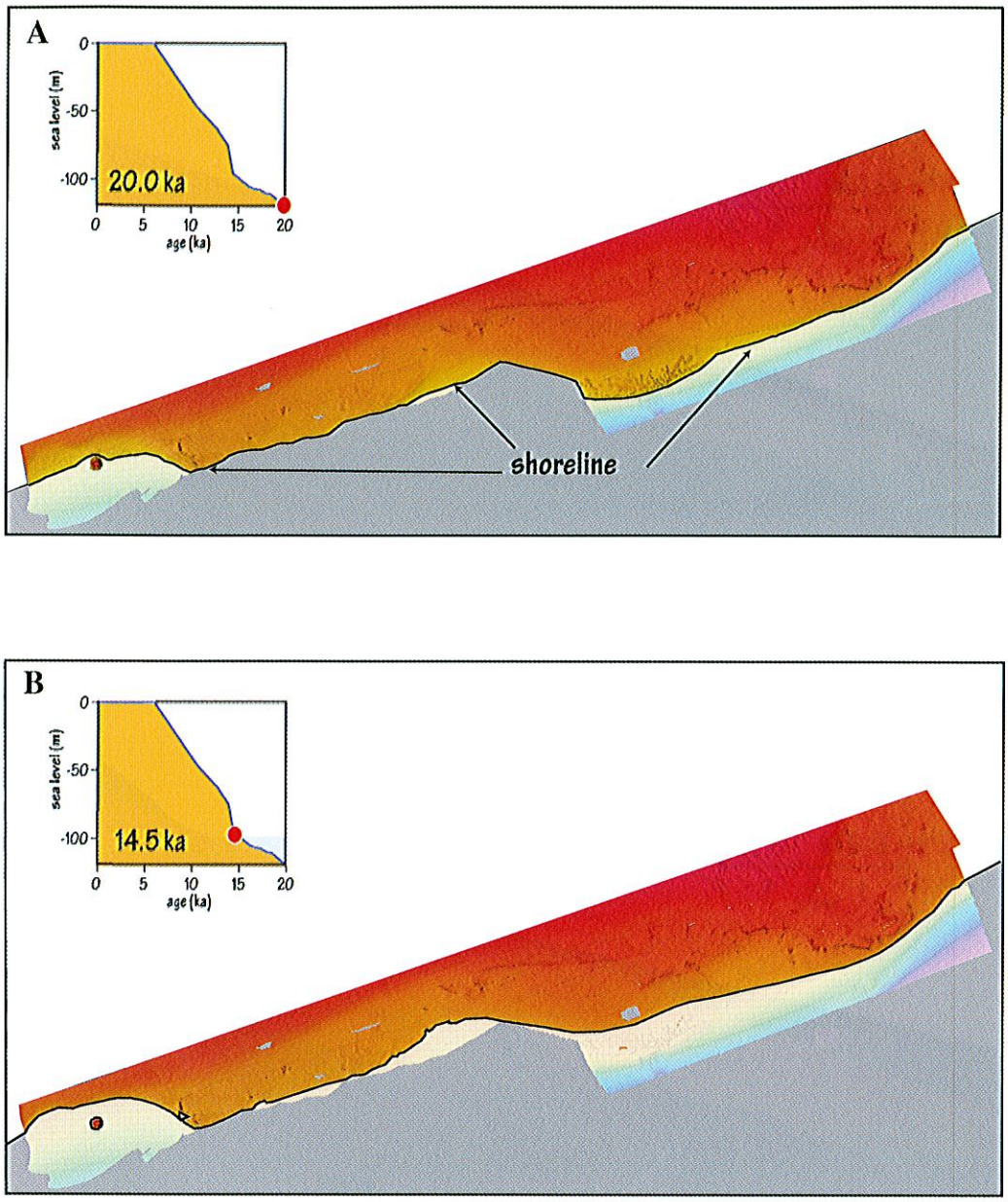

Fig. 20. Reconstructions of position of sea level at (A) 20 and 14.5 ka, demonstrating conditions conducive to reef formation and growth on outermost shelf; (B) position of sea level at 14.5 and 14.0 ka, showing affect of first melt-water pulse; (C) position of sea level at 14.0 and 12.0 ka, showing conditions conducive to reef formation and growth on midshelf; and (D) reconstructions of position of sea level at 12.0 and 11.0 ka, showing affect of second melt-water pulse. Diagram in upper left of each panel is age vs. sea level curve (Hanebuth et al., 2000), with red circle showing position of sea level at age indicated.

stand, then they can only represent exhumed cemented surfaces from an older period because, as beaches, many of them would have stood 25 to 40 m above sea level during the low stand. However, if the hardgrounds are a succession of cemented barrier islands or longshore bars formed during the latest Quaternary transgression, then a fundamental question is why did some of these beaches become cemented whereas others did not? An alter-

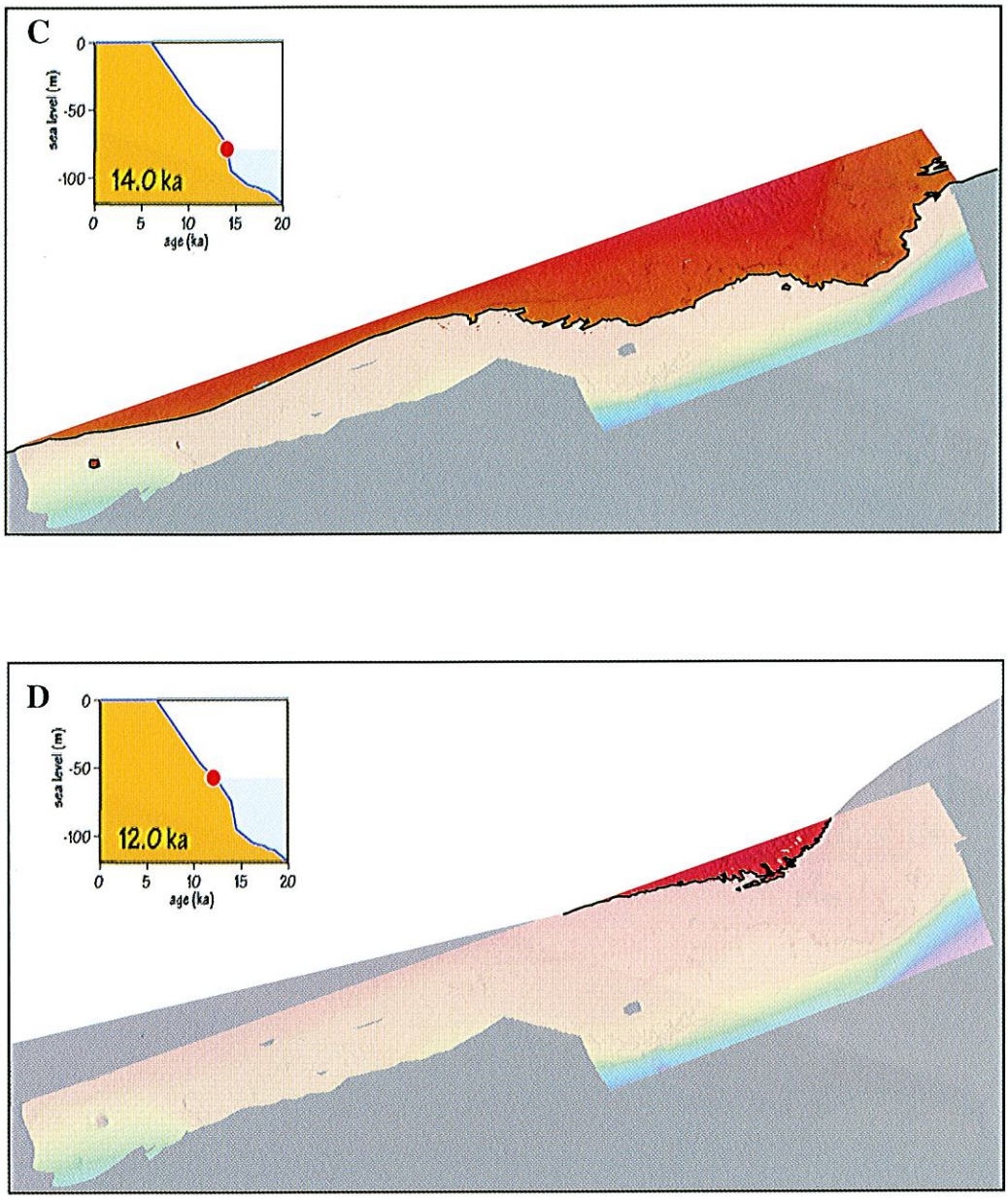

Fig. 20. Continued.

nate possibility is that the hardgrounds are sands cemented by the flow of freshwater and later exhumation.

Features related to the present eustatic high stand.— Most of the bedforms are asymmetrical with their stoss sides facing the southwest. This indicates that the bedforms are migrating to the northeast. However, the seafloor on the northeast side of almost all of the major features is consistently 3–5 m higher than the seafloor immediately to the southwest. This asymmetry suggests that the predominant sediment-transport direction over the duration of the eustatic high-stand has been toward the south and southwest. Almost all of the pinnacles and hardgrounds, as well as the prominent ridge, have moats on their southwest side. In addition, all of the large pinnacles, hardgrounds, and the ridge have a very high backscatter zone restricted to their tops and southwest sides, which suggests the presence of different material on either side of

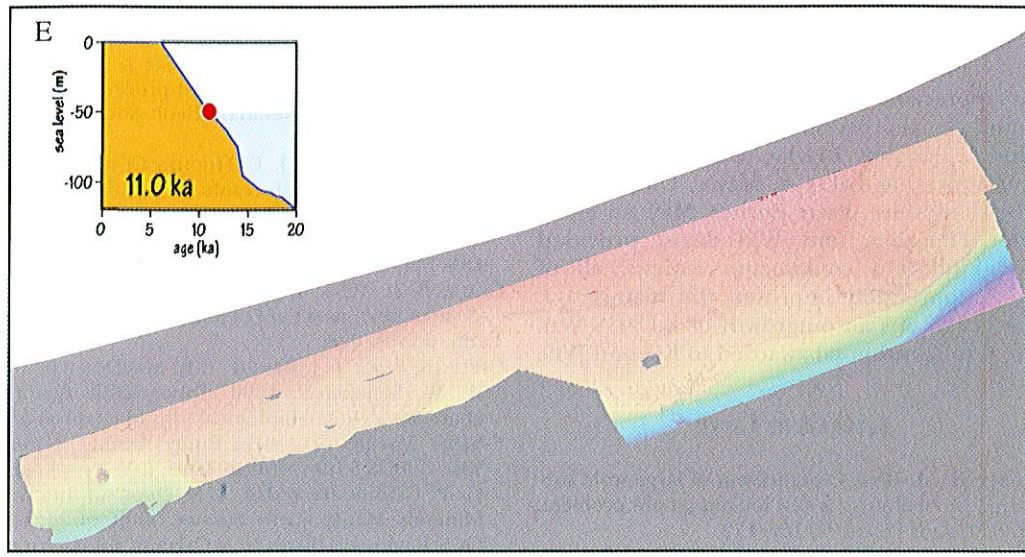

Fig. 20. Continued.

the features. The simplest explanation for these observations is that the bedforms are migrating under the influence of periodic excursions of the eastward-flowing Loop Current onto the shelf. The moats and high-backscatter zones suggest at least episodic aggressive bottom-water flow toward the southwest; turbulence generated by flow over the top of the features may have eroded the surface, swept eroded material off the bathymetric high, and created an erosional moat on the downstream side. The southwest direction of transport suggests that the extratropical cyclones (hurricanes) that pass through the northeast Gulf of Mexico must be the driving force for these erosion-related features. The hurricanes are intense low-pressure systems that generate very strong winds out of the northeast for several days at a time. It has been estimated that the average occurrence of hurricanes in this part of the Gulf of Mexico is 5–10 storms per year (Hayden, 1981). Although the erosion-related features could have initially been formed during the eustatic transgression, the features are fresh looking in the MBES data and lack the subdued morphology typical of relict features.

The shelf break has been modified by at least seven landslides. The causes of the landslides cannot be determined from the physiography alone, but several observations favor some mechanisms over others. The headwall of the landslide scar (LS1 in Fig. 1) is at the southern edge of a field of hardgrounds and pinnacles. The channel that leads away from the main landslide scar eventually evolves downslope into a broad area of failure. Two contradictory possibilities for the origin of the failure are suggested by these observations. The first possibility is that the failure was caused by sapping at the edge of the shelf. Although fields of pockmarks are found on the shelf and gas seepage is well documented in the Gulf of Mexico (for example, Bernard et al., 1976; Whelan et al., 1978; Brooks et al., 1979), there are no pockmarks in the vicinity of the shelf break nor in the areas of the shelf-edge landslides. Gas hydrates have been found in the northern Gulf of Mexico (Neurauter and Roberts, 1994; Neurauter and Bryant, 1989, 1990; Sassen et al., 1993, 1999; Milkov, 2000), although it is unlikely that the landslides are the result of a sublimated gas hydrate zone because the pressures and temperatures at the shelf break are not within the stability field that allows the formation of a hydrate. The second possibility is that an aquifer is exposed at the shelf edge and has discharged fluids that liquified the sediments of the shelf break, leading to failure. However, no freshwater discharge has been reported in the literature about this area. A third possibility is that the failure was caused by retrogressive failure initiated by failure lower on the slope (Fig. 16), and then successive upslope failures eroded up the slope to the shelf edge (Pratson and Coakley, 1996).

Acknowledgments

We would like to acknowledge the professionalism of the C&C Technologies, Inc. crew

aboard the RV *Ocean Surveyor*; in particular Art Kleiner, and the assistance and generosity of James and Thomas Chance. We also express our appreciation and gratitude for the post-cruise signal-processing advice provided by John E. Hughes Clarke, University of New Brunswick, and Larry A. Mayer, University of New Hampshire. Peter Barnes, Michael Field, Peter Fleischer, and Will Sager provided thoughtful and constructive reviews, all of which appreciably improved the manuscript. The cruise was an outgrowth of a USGS Venture Capital proposal awarded to KJS and JVG.

Literature Cited

Ashley, G. M. 1990. Classification of large-scale subaqueous bedforms: a new look at an old problem. J. Sediment Petrol. 60:160–172.

Benson, D. J., W. W. Schroeder, and A. W. Shultz. 1997. Sandstone hardbottoms along the western rim of DeSoto Canyon, northeast Gulf of Mexico. Trans. Gulf Coast Assoc. Geol. Soc. 47:43–48.

Bernard, B. B., J. M. Brooks, and W. M. Sackett. 1976. Natural gas seepage in the Gulf of Mexico. Earth Planet. Sci. Lett. 31:48–54.

Brooks, J. M., B. B. Bernard, W. M. Sackett, and J. R. Schwarz. 1979. Natural gas seepage on the south Texas shelf. Proc. Offshore Tech. Conf. 1: 471–178.

Carsey, J. B. 1950. Geology of Gulf coastal area and continental shelf. Bull. Am. Assoc. Petrol. Geol. 34:361–385.

CSA and TAMU (Continental Shelf Associates, Inc., and Texas A&M Univ.). 1999. Northeastern Gulf of Mexico coastal and marine ecosystem program: ecosystem monitoring, Mississippi/Alabama shelf; 3d Annual Interim Rep. U.S. Dept. of the Interior, U.S. Geological Survey, Biological Resources Division, USGS/BRD/CR-1999-0005 and Minerals Management Service, Gulf of Mexico OCS region, New Orleans, LA. OCS Study MMS 99-0055.

Diegal, F. A., D. C. Karlo, R. C. Schuster, R. C. Shoup, and P. R. Tauvers. 1995. Cenozoic structural evolution and tectono-stratigraphic framework of the northern Gulf Coast continental margin, p. 109–151. *In:* Salt tectonics: a global perspective. M. P. A. Jackson, D. G. Roberts, and S. Snelson (eds.). Am. Assoc. Petrol. Geol. Mem. 65.

Fairbanks, R. G. 1989. A 17,000-year glacio-eustatic sea level record: influence of glacial melting rates on the Yonger Dryas event and deep-ocean circulation. Nature 342:637–642.

Fleischer, P., and W. W. Schroeder. 1998. Hardbottoms on the inner continental shelf of Alabama and northwest Florida: interpretation and classification of side-scan sonar imagery. Miss. Acad. Sci., 62d Annual Meeting 43:57.

Fleming, K., P. Johnston, D. Zwartz, Y. Yokoyama, K. Lambeck, and J. Cahppell. 1998. Refining the eustatic sea-level curve since the Last Glacial Maximum using far- and intermediate-field sites. Earth Planet. Sci. Lett. 163:327–342.

Gardner, J. V., L. A. Mayer, and J. E. Hughes Clarke. 2000. Morphology and processes in Lake Tahoe (California-Nevada). Geol. Soc. Am. Bull. 112:736–746.

———, L. A. Mayer, J. E. Hughes Clarke, and A. Kleiner. 1999. High-resolution multibeam bathymetry of East and West Flower Gardens and Stetson Banks, Gulf of Mexico. Gulf Mex. Sci. 16: 131–143.

Gealy, B. L. 1955. Topography of the continental slope in northwest Gulf of Mexico. Bull. Geol. Soc. Am. 66:203–228.

Gittings, S. R., T. J. Bright, I. R. MacDonald, and W. W. Schroeder. 1990. Topographic features characterization—biological. *In:* Mississippi-Alabama Marine Ecosystem Study Annual Report, Year 2. OCS Study, MMS-89-0095. J. M. Brooks and C. P. Giammona (eds.). U.S. Dept. of Interior, Minerals Management Service, Gulf of Mexico OCS Regional Office, New Orleans, LA. Contract No. 14-12-0001-30346.

Grigg, R. W., and D. Epp. 1989. Critical depth for the survival of coral islands: effects on the Hawaiian Archipelago. Science 243:638–641.

Hanebuth, T., K. Stattegger, and P. M. Grootes. 2000. Rapid flooding of the Sunda shelf: a late-glacial sea-level record. Science 288:1033–1035.

Hayden, B. P. 1981. Secular variation in Atlantic coast extratropical cyclones. Mon. Weather Rev. 109:159–167.

Hilde, T. W. C., R. L. Carlson, A. F. Gangi, M. C. Lee, S. F. Dwan, C. W. Kue, C. H. Herrick, P. Devall, P. Alleman, C. J. Sonnier, J. Moore, T. Richards, J. Ross, and R. Miller. 1991. [TAMU]^2: new generation seafloor mapping technology. Sea Technol. 32:37–40.

Hovland, M., and A. G. Judd. 1988. Seabed pockmarks and seepages. Graham and Trotman, London.

Hughes Clarke, J. E., L. A. Mayer, and D. E. Wells. 1996. Shallow-water imaging multibeam somars: a new tool for investigating seafloor processes in the coastal zone and on the continental shelf. Mar. Geophys. Res. 18:607–629.

Kindinger, J. L. 1988. Seismic stratigraphy of the Mississippi-Alabama shelf and upper continental slope. Mar. Geol. 83:79–94.

———. 1989. Depositional history of the Lagniappedelta, northern Gulf of Mexico. Geo-Mar. Lett. 9:59–66.

Laswell, J. S., W. W. Sager, W. W. Schroeder, K. S. Davis, and R. Rezak. 1994. High resolution geophysical mapping of the Mississippi-Alabama outer continental shelf, p. 155–192. *In:* Handbook of geophysical exploration at sea. 2d ed. Hard minerals. R. A. Geyer (ed.). CRC Press, Boca Raton.

———, ———, ———, R. Rezak, K. S. Davis, and E. G. Garrison. 1990. Atlas of high-resolution geophysical data, Mississippi-Alabama Marine Ecosystem Study. OCS Study/MMS 90-0000. U.S. Dept. of the Interior, Minerals Mgmt. Service, Gulf of Mexico OCS Regional Office, New Orleans, LA.

———, W. W. SCHROEDER, AND W. W. SAGER. 1991. Seafloor acoustic backscatter on the Mississippi-Alabama outer continental shelf. Trans. Gulf Coast Assoc. Geol. Soc. 44:373–379.

LUDWICK, J. C. 1964. Sediments in northeastern Gulf of Mexico, p. 204–238. *In:* Papers in marine geology, Shepard commemorative volume. R. L. Miller (ed.). The Macmillan Co., New York.

———, AND W. R. WALTON. 1957. Shelf-edge, calcareous prominences in northeastern Gulf of Mexico. Bull. Am. Assoc. Petrol. Geol. 41:2054–2101.

MARTIN, R. G. 1978. Northern and eastern Gulf of Mexico continental margin: stratigraphic and structural framework, p. 21–42. *In:* Framework, facies, and oil-trapping characteristics of the upper continental margin. A. H. Bouma, G. T. Moore, and J. M. Coleman (eds.). Am. Assoc. Petroleum Geol. Stud. Geology, 7. American Association of Petroleum Geologists, Tulsa.

MAZZULLO, J., AND C. BATES. 1985. Sources of Pleistocene and Holocene sand for the northeast Gulf of Mexico shelf and the Mississippi Fan. Trans. Gulf Coast Assoc. Geol. Soc. 35:457–465.

MCBRIDE, R. A., AND M. R. BYRNES. 1995. Surficial sediments and morphology of the southwestern Alabama/western Florida panhandle coast and shelf. Trans. Gulf Coast Assoc. Geol. Soc. 45:393–404.

MILKOV, A. V. 2000. Worldwide distribution of submarine mud volcanoes and associated gas hydrates. Mar. Geol. 167:29–42.

MOLINARI, R. L., AND D. A. MAYER. 1982. Current meter observations on the continental slope at two sites in the eastern Gulf of Mexico. J. Phys. Ocean. 12:480–484.

NEURAUTER, T. W., AND W. R. BRYANT. 1989. Gas hydrates and their association with mud diapers/mud volcanoes on the Louisiana continental slope. Proc. Offshore Tech. Conf. 1:599–607.

———, AND ———. 1990. Seismic expression of sediment volcanism on the continental slope, northern Gulf of Mexico. Geo-Mar. Lett. 10:225–231.

———, AND H. H. ROBERTS. 1994. Three generations of mud volcanoes on the Louisiana continental slope. Geo-Mar. Lett. 14:120–125.

NOAA. 1998. NOS hydrographic survey data. National Ocean. and Atmos. Admin. World Data Center for marine geology and geophysics, CD-ROM 98-MGG-03.

PARKER, R. H., AND J. R. CURRAY. 1955. Macrofauna and bathymetry of calcareous banks on the continental shelf of the northern Gulf of Mexico (abstract). Bull. Geol. Soc. Am. 66:1604–1605.

PRATSON, L. F., AND B. J. COAKLEY. 1996. A model for the headward erosion of submarine canyons induced by downslope-eroding sediment-flows. Geol. Soc. Am. Bull. 108:225–234.

SAGER, W. W., W. W. SCHROEDER, K. S. DAVIS, AND R. REZAK. 1999. A tale of two deltas: seismic mapping of near surface sediments on the Mississippi-Alabama outer shelf and implications for recent sea level fluctuations. Mar. Geol. 160:119–136.

———, ———, J. S. LASWELL, K. S. DAVIS, R. REZAK, AND S. R. GITTINGS. 1992. Mississippi-Alabama outer continental shelf topographic features formed during the late Pleistocene-Holocene transgression. Geo-Mar. Lett. 12:41–48.

SASSEN, R., J. M. BROOKS, I. R. MACDONALD, M. C. KENNICUTT, N. L. GUINASSO, AND A. G. REQUEJO. 1993. Association of oil seeps and chemosynthesis communities with oil discoveries, upper continental slope, Gulf of Mexico. Trans. Gulf Coast Assoc. Geol. Soc. 43:349–355.

———, S. JOYE, S. T. SWEET, D. A. DEFREITAS, A. V. MIKLOV, AND I. R. MACDONALD. 1999. Thermogenic gas hydrates and hydrocarbon gases in complex chemosynthetic communities, Gulf of Mexico continental slope. Org. Geochem. 30:485–497.

SCHROEDER, W. W., D. J. BENSON, P. FLEISCHER, AND S. R. GITTINGS. 1997. The role of geomorphology, benthic boundary layer processes and fluvial influence in structuring continental shelf hardbottom habitats in the northeastern Gulf of Mexico [Abstract]. Geol. Soc. Am. Abst. Programs, p. A-257. Geological Society of America, Boulder.

———, A. W. SHULTZ, AND J. J. DINDO. 1988. Inner-shelf hardbottom areas, northeastern Gulf of Mexico. Trans. Gulf Coast Assoc. Geol. Soc. 38:535–541.

SHEPARD, F. P. 1937. Salt domes related to Mississippi submarine troughs. Bull. Geol. Soc. Am. 48:1349–1362.

TROWBRIDGE, A. K. C. 1930. Building of Mississippi Delta. Bull. Am. Assoc. Petrol. Geol. 14:867–901.

VOKOVICH, F. M. 1988. Loop Current boundary variations. J. Geophys. Res. 93:15,585–15,591.

WHELAN, T., J. T. ISHMAEL, AND G. G. RAINEY. 1978. Gas-sediment interactions in Mississippi Delta sediments. Proc. Offshore Tech. Conf. 2:1029–1036.

(JVG, PD) U.S. GEOLOGICAL SURVEY, MENLO PARK, CALIFORNIA 94025; (KJS) U.S. GEOLOGICAL SURVEY, GAINESVILLE, FLORIDA; (BC, LH) UNIVERSITY OF NEW HAMPSHIRE, DURHAM, NEW HAMPSHIRE. Date accepted: September 7, 2001.